2006

Scaffold Permeability as a Means to Determine Fiber Diameter and Pore Size of Electrospun Fibrinogen

Scott Allen Sell
Virginia Commonwealth University

School of Engineering
Virginia Commonwealth University

This is to certify that the thesis prepared by Scott Allen Sell entitled SCAFFOLD PERMEABILITY AS A MEANS TO DETERMINE FIBER DIAMETER AND PORE SIZE OF ELECTROSPUN FIBRINOGEN has been approved by his committee as satisfactory completion of the thesis or dissertation requirement for the degree of Masters of Science in Biomedical Engineering

Gary L. Bowlin, Ph.D., School of Engineering

David G. Simpson, Ph.D., School of Medicine

Paul A. Wetzel, Ph.D., School of Engineering

Gerald E. Miller, Ph.D., Chair of Biomedical Engineering, School of Engineering

L. Thomas Overby, Ph.D., Assistant Dean of Graduate Affairs, School of Engineering

Russell D. Jamison, Ph.D., Dean, School of Engineering

F. Douglas Boudinot, Ph.D., Dean of the School of Graduate Studies

Date

SCAFFOLD PERMEABILITY AS A MEANS TO DETERMINE FIBER DIAMETER AND PORE SIZE OF ELECTROSPUN FIBRINOGEN

A thesis submitted in partial fulfillment of the requirements for the degree of Masters of Science in Biomedical Engineering at Virginia Commonwealth University.

by

SCOTT ALLEN SELL
B.S., Virginia Commonwealth University, 2003

Director: GARY L. BOWLIN, PH.D
ASSOCIATE PROFFESOR, BIOMEDICAL ENGINEERING

Virginia Commonwealth University
Richmond, Virginia
August, 2006

Acknowledgement

This has been a long time in coming, much longer than originally anticipated, and therefore requires the thanking of the many people who pushed, carried, and occasionally drug me through it all. Of course I would have to start by thanking Dr. Gary Bowlin, my advisor and perennial lunch date. Aside from the obvious thanks for advisor type things, thanks for looking out for me and providing me with some focus. I am not afraid to say that at points in my life I felt like I was just drifting along without direction. Thanks to Dr. David Simpson, whose sense of humor and blatant disregard for authority made trips to Sanger Hall's ninth floor both informative and comical. Many thanks to my lab mates, particularly Catherine Barnes, who patiently listened to every harebrained idea I had in the last three years. My parents deserve a large portion of thanks for carrying me along as far as they did. Finally, I would like to offer my most sincere thanks to my wife, Tracy, who essentially made all of this possible by supporting and pushing me for longer than I can remember. I promise I will get a job at some point!

Table of Contents

Page

Acknowledgements ii

List of Tables v

List of Figures vi

Chapter

1 **Introduction** 1

Project Synopsis 2

2 **Background Information** 3

Tissue Engineering 3

Native ECM 5

ECM Analogue Scaffolds 7

Porosity, Permeability, and Diffusion: Their Role in Tissue Engineering 10

Nanofibrous Scaffold Fabrication Techniques 12

Electrospinning 15

3 **Materials and Methods** 19

Electrospinning 19

Scaffold Characterization 20

Flowmeter Design 21

Test of Flowmeter Efficacy 27

Permeability Measurement 28

Permeability Based Fiber Diameter and Pore Size 30

Statistical Analysis 31

4 **Results** 32

Scaffold Characterization 32

Test of Flowmeter Efficacy 37

Permeability Measurement 37

Permeability Based Fiber Diameter and Pore Size 44

5 **Discussion** 49

Scaffold Characterization 49

Permeability Measurement 50

Permeability Based Fiber Diameter and Pore Size 54

6 **Conclusion** 57

References 59

Appendix 64

A Tables of statistically significant differences of fiber and pore sizes 64

List of Tables

Page

Table 1: Some major ECM components, their function, and location.....6

Table 2: Table of specimen mount components. 27

Table 3: Average fiber and pore diameters of electrospun scaffolds determined with ImageTool. 33

Table 4: Average fiber and pore diameters of electrospun scaffolds determined by both ImageTool analysis and permeability based calculations. 45

List of Figures

Page

Figure 1: Cell-ECM integrin binding.....7

Figure 2: Diffusional distances of various small molecules.....11

Figure 3: Transmission electron micrograph of fibers formed through self-assembly.....14

Figure 4: Nanofibrous PLLA scaffold formed through phase separation.....15

Figure 5: Generic electrospinning setup.....16

Figure 6: Photograph of an electrospun fibrinogen scaffold. 17

Figure 7: Diagram of a simple flowmeter design for measuring fibrin gel permeability..22

Figure 8: Photograph of electrospun scaffold specific flowmeter.....23

Figure 9: Measurement portion of electrospun scaffold flowmeter.....24

Figure 10: Specimen mount portion of electrospun scaffold flowmeter 25

Figure 11: Exploded view of flowmeter specimen mount.....26

Figure 12: Scanning electron micrographs of dry fibrinogen scaffolds 34

Figure 13: Scanning electron micrographs of hydrated fibrinogen scaffolds.....35

Figure 14: Line graph of average fiber and pore diameters versus fibrinogen concentration.....36

Figure 15: Photographic evidence of flowmeter efficacy.....37

Figure 16: Graph of average scaffold volume fraction versus fibrinogen concentration ..38

Figure 17: Line graph of average scaffold permeability versus time for the first ten minutes of testing.....40

Figure 18: Graph of average scaffold permeability versus fibrinogen concentration 42

Figure 19: Line graph of average scaffold permeability versus fibrinogen concentration depicting the linear relationship between the two.....43

Figure 20: Graph of average electrospun scaffold fiber diameters determined by permeability based equations and image analysis 46

Figure 21: Graph of average electrospun scaffold pore diameters determined by permeability based equations and image analysis 48

Abstract

SCAFFOLD PERMEABILITY AS A MEANS TO DETERMINE FIBER DIAMETER AND PORE SIZE OF ELECTROSPUN FIBRINOGEN

By Scott Allen Sell, B.S.

A thesis submitted in partial fulfillment of the requirements for the degree of Masters of Science in Biomedical Engineering at Virginia Commonwealth University.

Virginia Commonwealth University, 2006

Major Director: Gary L. Bowlin, Ph.D.
Associate Professor, Biomedical Engineering

The purpose of this study was to construct a flowmeter that could accurately measure the hydraulic permeability of electrospun fibrinogen scaffolds, providing insight into the transport properties of electrospun scaffolds while making the measurement of their topographical features (fiber and pore size) more accurate. Three different concentrations of fibrinogen were used (100, 120, and 150mg/ml) to create scaffolds with three different fiber diameters and pore sizes. The fiber diameters and pore sizes of the electrospun scaffolds were analyzed through scanning electron microscopy and image

analysis software. The permeability of each scaffold was measured and used to calculate permeability-based fiber diameters and pore sizes, which were compared to values obtained through image analysis. Permeability measurement revealed scaffold permeability to increase linearly with fibrinogen concentration, much like average fiber diameter and pore size. Comparison between the two measurement methods proved the efficacy of the flowmeter as a way to measure scaffold features.

Introduction

The interdisciplinary field of tissue engineering has blossomed in the brief two decades since the term was coined. While extensive research has been done in many areas that would fall under the umbrella name of tissue engineering, of particular interest to this study is the research done on the creation of scaffolds that mimic the native extracellular matrix. A countless number of materials and processing techniques have been used to engineer these extracellular matrix analogues, with varying degrees of success. Although scaffolds may be designed and created to fit a specific application, ultimately all scaffolds regardless of application must meet a number of basic criteria to be successful. At its most fundamental, the scaffold should not elicit an immune response while remaining a viable framework for cellular infiltration/proliferation. At first glance an elementary task, this requires the scaffold to have an idealized combination of mechanical properties, geometry, and surface chemistry. Altered scaffold permeability and nutrient/waste diffusion, important in their own rite, can be a byproduct of tailoring the aforementioned scaffold characteristics. The purpose of this study was to construct a flowmeter that could accurately measure the hydraulic permeability of electrospun fibrinogen scaffolds of varying fiber diameter and alignment. This permeability would then be used to calculate average fiber diameters and pore areas for comparison with values determined by image analysis software. Based on previous work, scaffolds composed of smaller diameter fibers should be less permeable than those composed of larger diameter fibers, as smaller fibers

result in smaller pore areas, less void space, and overall greater tortuosity. Fiber alignment should also have an effect on scaffold permeability as randomly aligned fibers would present a more tortuous path than oriented fibers, resulting in decreased permeability.

Project Synopsis

This study explores the effects of fiber diameter and orientation on the hydraulic permeability of electrospun fibrinogen scaffolds, while using permeability to determine average fiber diameters and pore sizes. The percentage void space was determined for each of the electrospun samples in both a dry and hydrated state. A flowmeter was designed and constructed to accurately measure the permeability of said samples, from which average fiber diameters and pore areas were calculated. These calculated values were then compared to values that were determined using image analysis software. The major purpose of this study was to create a device that easily and accurately measures electrospun scaffold permeability that could be used in future research. In addition the quantification of electrospun fibrinogen scaffold permeability would provide further insight into the transport properties, geometry, and behavior of generic electrospun scaffolds, while allowing for more accurate representations of their average fiber diameters and pore sizes.

Background Information

Tissue Engineering

Tissue engineering is an interdisciplinary field that was generically defined in 1988 as the application of principles and methods of engineering and life sciences toward the fundamental understanding of structure-function relationships in normal and pathological mammalian tissues and the development of biological substitutes to restore, maintain, or improve tissue functions [1, 2]. Typically this involves collaborative efforts between materials scientists, cell and molecular biologists, immunologists, surgeons, and engineers to create tissue engineered medical products (TEMPs) [2, 3]. These TEMPs fall into one of three different categories: 1) isolated cells or cell substitutes, 2) tissue-inducing substances, 3) and cells placed on or within a matrix.

The first category, isolated cells or cell substitutes, is the most direct tissue engineering approach typically using autologous or allogenic cells as therapeutic agent. This allows for the replacement of cells in areas of damaged tissue, ultimately using the cell's ability for replication to promote tissue repair and resumed function [2, 4]. These cells can be differentiated and tissue specific (i.e. injecting chondrocytes in cartilage) or can be undifferentiated, generic stem cells that could be injected into areas of damaged tissue and allowed to differentiate as needed [3]. The upside of such an approach is the

avoidance of surgery, as well as the ability to manipulate cells as needed *in vitro* prior to their implantation into the body. However, the major drawback of this approach is the time required to culture a usable number of cells. Without the presence of a large universal cell bank, cells must be taken from a donor and cultured to a usable number prior to implantation in their eventual recipient [3, 4].

The use of tissue-inducing substances relies on the cells already in place within a patient's body, however these cells are augmented by the introduction of additional signaling molecules. These signaling molecules can include a wide number of cytokines and chemokines to promote cell growth, instruct differentiation, and promote cellular migration [2]. One of the downsides to this approach is the reliance upon cells that are residing within a degraded environment; if the patient were healthy they would not need this treatment. The remaining cells may not have the capacity to regenerate the area of concern. Another problem is the containment of these signaling molecules to the site of interest. A number of drug delivery systems have been tried with varying degrees of success to deliver signaling molecules to their destination [4].

The use of cells placed on or within a matrix may be the most challenging, albeit potentially the most beneficial, approach to tissue engineering. These matrix-based approaches can be further divided into closed systems and open systems. Closed systems are kept separate from the body, and away from the immune system, by a membrane that allows for transport of nutrients and waste while protecting the cells and other constituents from antibodies and immune cells. Open systems are implanted directly into the body in hopes that they become incorporated directly into normal physiological functioning of the

tissue. These systems are meant to mimic the native extracellular matrix (ECM) and can serve as a structural framework for both cells and signaling molecules. The idea being that through physical and chemical induction, the ECM analogue will induce cells to more accurately reproduce their normal physiological behavior, thereby improving tissue regeneration and repair [5]. Since they are open to immunological attack, much research has been done on the material composition of open matrix systems, in order to produce matrices that elicit little to no immune response. For this reason most matrices are composed of either synthetic polymers such as poly(glycolic acid) (PGA), or natural polymers like collagen [4].

Native ECM

Most mammalian tissue is composed of two major components: cells and ECM. A majority of tissue volume is composed of the ECM component, which also provides much of a tissue's geometric shape. From a structural standpoint, the ECM is a complex arrangement of proteins and polysaccharides such as collagen, hyaluronic acid, proteoglycans, glycosaminoglycans, and elastin. These ECM components are constantly being synthesized, secreted, oriented, and modified by the cellular components that they support. Classically the function of native ECM was only believed to be as a structural framework for tissues. However the ECM, through interaction with receptors on the surfaces of cells, directly takes part in promoting cell adhesion, migration, growth,

differentiation, and apoptosis. The ECM also plays a role in cytokine activity and intracellular signaling. Growth factors and signaling molecules can be stored within ECM to preserve against their degradation, or they can attach to the surface of the ECM to present themselves more efficiently to cell receptors [2, 6].

Table 1: Some major ECM components, their function, and location. Adapted from [2].

Component	Function	Location
Collagen	Tissue architecture, tensile strength, cell-matrix interaction, matrix-matrix interaction	Widely distributed
Elastin	Tissue architecture, elasticity	Tissues requiring elasticity (lung, blood vessel, skin)
Proteoglycans	Cell-matrix interaction, matrix-matrix interaction, cell proliferation, cell migration	Widely distributed
Hyaluronan	Cell-matrix interaction, matrix-matrix interaction, cell proliferation, cell migration	Widely distributed
Laminin	Basement membrane component, cell migration	Basement membranes
Fibronectin	Tissue architecture, cell-matrix interaction, matrix-matrix interaction, cell proliferation, cell migration	Widely distributed
Fibrinogen	Cell proliferation, cell migration, hemostasis	Blood, wound healing

Interactions between cells and the ECM are complex and dynamic, and play critical roles during development and wound healing. During development, cell-ECM interaction is responsible for pattern formation, morphogenesis, and phenotype acquisition and maintenance. During wound healing clot formation, inflammation, formation of granulation tissue, and remodeling are all mediated by cell-ECM interaction. Heterodimeric transmembrane proteins known as integrins on the cell surface bind to specific small peptide fragment sequences on the ECM molecules allowing for cells to

bind to the ECM and promote direct communication between the two. Signals are sent from the ECM across the cell membrane to soluble molecules in the cytoplasm and through direct connections with the cytoskeleton and into the cell nucleus, evoking a cellular response. This direct contact allows for stronger, more specific signaling than through the release of diffusible signaling molecules. In what is known as dynamic reciprocity, the cellular response to the ECM signaling can often alter the state of the ECM. For example cells may release matrix metalloproteases to break down an overly dense ECM to allow for their migration or proliferation [2, 6].

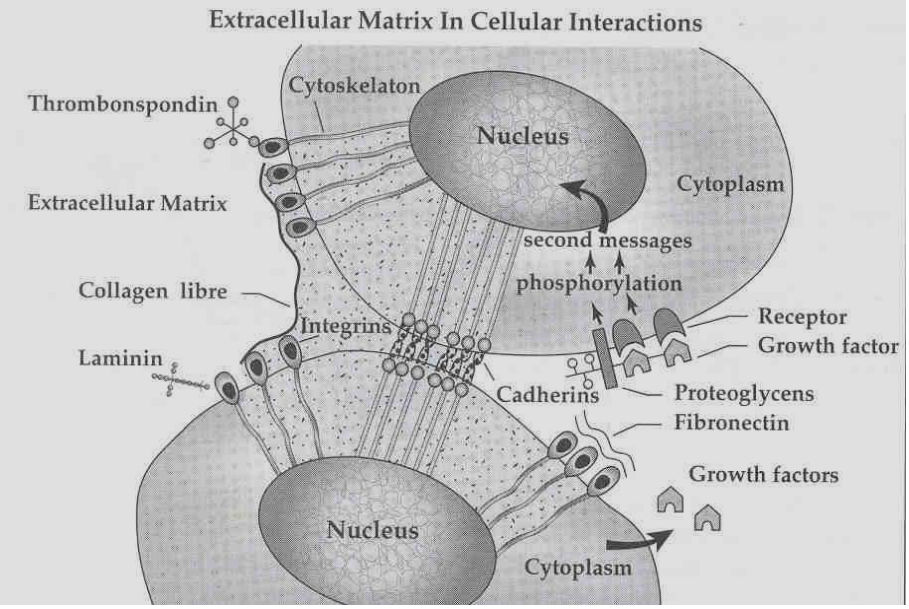

Figure 1. Diagram of cell-ECM interactions through both integrin binding and signaling molecules. Notice with integrin binding ECM signals are transmitted from the integrin binding site to the cell nucleus via cytoskeletal elements [2].

ECM Analogue Scaffolds

As complex a structure as the native ECM has been revealed to be, it should be no surprise that the creation of a successful engineered ECM analogue has proven to be extremely challenging. Ideally, one would like to mimic both the fibrillar form and the complex function of the native ECM [7-9]. To attain a successful ECM analogue scaffold, there are several design and material criteria that must be met. First and foremost, the scaffolding material should be subjected to the same standards as any other biomaterial implanted in the body, namely, the scaffold should not initiate any adverse tissue or immune reactions. For many applications, scaffolding materials should be biodegradable or bioabsorbable at a rate that will allow for their gradual incorporation into the surrounding tissue without any fibrous encapsulation or residual evidence of their presence [7, 8]. A wide number of different polymers, both synthetic and natural in origin, have been used as ECM analogue scaffolding. The most common synthetic polymers in use today remain PGA, poly(lactic acid) (PLA), and their copolymers. However there has also been work done with polycaprolactone (PCL), as well as some polyanhydrides, polyorthoesters, polycarbonates, and polyfumarates [7]. As for ECM analogues engineered from natural materials, collagens [10], elastin [11], and fibrinogen [12] have been used. ECM substitutes of this variety have the potential for a greater upside than their synthetic counterparts due to the fact that they are constructed from native ECM materials and may be expected to retain some of their biologic behavior [13].

The architecture of the scaffold is every bit as important as the material from which it is fabricated. As previously stated, an ECM analogue should mimic the form of the native ECM. To be ideal, this ECM analogue would need to mimic the topographical features and geometry on the macro-scale, micro-scale, and even nano-scale levels, as each influences cell response to the scaffold [14]. Native ECM is composed of nanoscale fibers that offer structural integrity to tissues. Recent advances in fabrication techniques have made the creation of consistent nanofiber scaffolds possible. The use of nanofibrous scaffolds creates structures with a very high surface area to volume ratio to support cell growth and infiltration [9, 15]. In addition, the morphological similarities between the nanofibrous structures and the native ECM are believed to improve cellular response and overall biocompatility [9].

Success as a tissue-engineering scaffold in many applications is ultimately dependant upon the ability for cells to infiltrate the ECM analogue, migrate throughout its thickness, and proliferate [16, 17]. The scaffold's porous structure, a combination of microporous (pore diameters < 2 nm), mesoporous (pores with diameter 2 nm – 50 nm), or macroporous (pore diameters > 50 nm) void spaces, plays a major role in cellular penetration [13, 18]. There has been no concrete claim to an ideal pore diameter, yet there is a definite threshold to tissue ingrowth. It has been shown that tissue will not grow in pores smaller than 5 μm in diameter. Pores 5-15 μm in diameter will support fibrous tissue growth, while osteoid tissue requires pores 40-100 μm in diameter, and still larger pores ranging from 100-400 μm are needed for the successful mineralization of bone. Not only do the pores of an ECM analogue scaffold need to be of a specific size for tissue growth to

occur, but they also need to be open and interconnected. Interconnectivity refers to the extent of which pores are connected with their neighboring pores, and has a large effect on nutrient and waste diffusion, cell migration, and overall scaffold permeability [19, 20]. The importance of diffusion and permeability to tissue engineering will be discussed in detail in the following section.

Porosity, Permeability, and Diffusion: Their Role in Tissue Engineering

The terms porosity and permeability are often incorrectly used interchangeably in the realm of tissue engineering and in the consideration of ECM analogue scaffolds. By definition, porosity is the amount of void space contained within a structure, while permeability is a measure of the ease of which a fluid can move through the structure. The porosity of a scaffold can have a large effect on the scaffold's permeability. Generically speaking, an increase in scaffold porosity will lead to an increase in scaffold permeability. However, this ultimately depends on the combination of scaffold porosity, pore size and distribution, pore interconnectivity, and pore orientation and scaffold tortuosity to determine the hydraulic permeability of an ECM analogue scaffold [19, 20].

While not often reported, scaffold permeability and porosity are of extreme importance to tissue engineering. Healthy, living tissue *in vivo* relies on the microvasculature to distribute blood and exchange metabolites through a combination of diffusion over short distances and flow-limited exchange. There are currently no tissue

engineered products that contain their own prevascularised capillary bed to provide nutrients to the structure, chaining their initial effectiveness to the limits of passive diffusion [21]. The limitations of diffusion based nutrient transport (see figure 2) restrict the maximum thickness of avascular tissue engineered constructs to less than 2 mm [22]. Scaffolds with increased porosity and permeability help to promote the diffusion of nutrients to cellular constituents, while promoting the diffusion of metabolic waste away from the cells. An increase in nutrient penetration distance will promote cell migration away from the scaffold periphery, and the presence of interconnected macropores will augment their ability to migrate [19, 20]. The degradation behavior of synthetic polymer based scaffolds is also controlled in part by the permeability of the ECM analogue. Low porosity and permeability scaffolds made of poly(α-hydroxy acids) have exhibited increased rates of degradation due to an increase in autocatalytic activity. Essentially, as the polymers breakdown via hydrolysis, the acidic byproducts become trapped within the scaffold and lower the local pH. This reduced pH then accelerates the degradation of the polymer from the inside out resulting in a rapid loss of mechanical stability [19, 23].

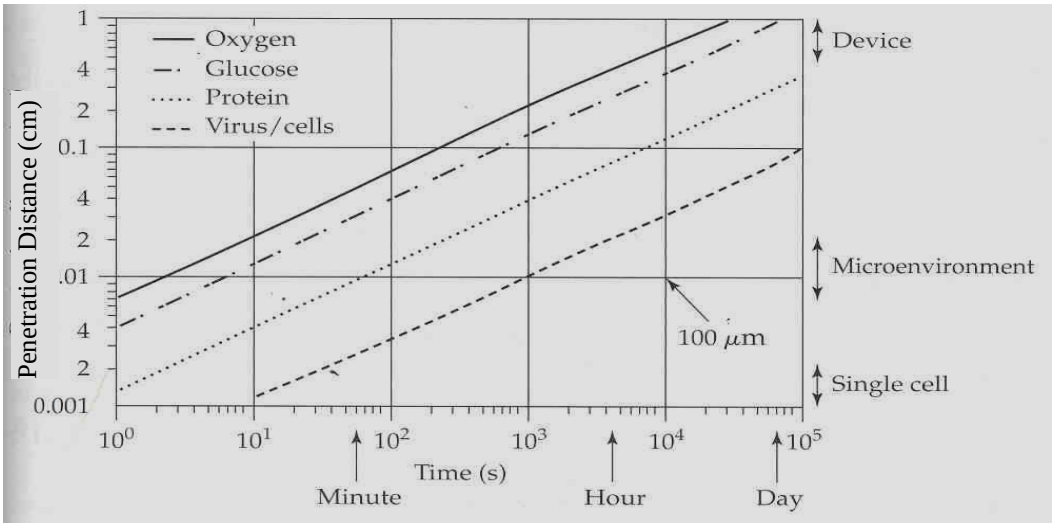

Figure 2. Graph of the diffusional distance of a number of different molecules necessary for cellular survival as a function of time. The smaller a molecule is, the faster it will move by diffusion. For example, larger molecules such as proteins diffuse shorter distances than small molecules like oxygen [2].

While permeability and porosity may be essential to scaffold success, engineers must balance efficient nutrient diffusion and cell migration with desirable mechanical stability, as increased porosity leads to a decrease in mechanical properties. As such, it has been suggested that the most pragmatic way to present permeability and porosity information is to use a permeability/porosity ratio. This ratio acts as an indicator of the scaffolds percolative efficiency per unit porous volume [19, 20].

Nanofibrous Scaffold Fabrication Techniques

There are currently a wide number of scaffold processing techniques employed for the creation of ECM analogue scaffolds. Some of the more popular being fiber bonding [8,

24], solvent casting and particulate leaching [8, 25], gas foaming [8, 26, 27], and rapid prototyping techniques [8, 28]. These methods each have their pros and cons; particulate leaching offers excellent control over pore size, while rapid prototyping provides great control over spacing and orientation. However, none of these methods has the ability to create nanofibrous structures that mimic the 50-500 nm diameter fibers that make up the native ECM [29]. Three distinct scaffold fabrication methods have been proven to create sub-micron scale fibers on a routine basis: self-assembly, phase separation, and electrospinning. Self-assembly and phase separation will be discussed briefly in this section, while electrospinning will be discussed in detail in the following section as it is the method of choice for this lab, and the method utilized for this study.

Self-assembly is essentially putting into laboratory practice a process that occurs naturally in nucleic acid synthesis, protein synthesis, and energy transduction. This process is limited to use with a select few polymers, the most common of which are peptide-amphiphiles (PA). These PAs contain a long hydrophobic alkyl tail, that when placed in water will form a PA cluster known as a cylindrical micelle. One of three different self-assembly procedures will then be employed to create fibers from the micelle clusters. For acid induced self-assembly, the micelles are treated with a dithiothreitol solution of pH 8 where the PA remains soluble. The pH is then rapidly reduced to 4 to make the PA insoluble, producing fibers. Divalent ion induced self-assembly uses the addition of Ca^{2+} ions to cause gelation, while the drying on surfaces procedure is simply allowing the pH 8 water solution to dry on a surface. On average these self-assembly procedures produce fibers 5-8 nm in diameter and 1 μm in length. While nanofibers are

successfully created, self-assembly is limited by the complexity of the procedure and the low end-product yield [8, 29-32].

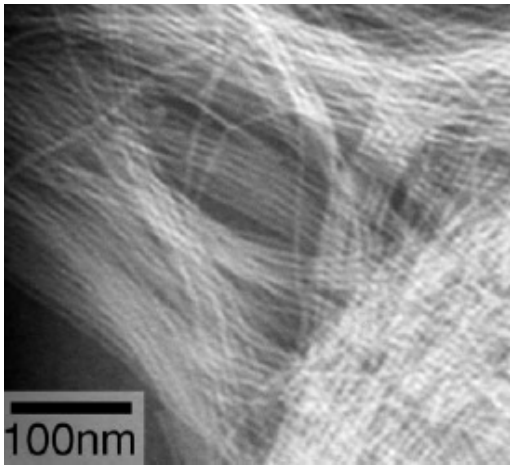

Figure 3. Transmission electron micrograph of fibers formed through self-assembly. The fibers depicted have diameters between 5 and 8 nm and a length of 1 μm [32].

Phase separation is a method to produce ECM analogue scaffolds that offers engineers a large amount of control over the macroporous architecture, while still creating fibers that range in diameter from 50-500 nm. Phase separation works on the principal of thermodynamically separating a polymer-rich component from a polymer-poor component. An aliphatic polyester is dissolved in solution and phase separation is induced thermally or through the addition of a nonsolvent to create a gel. Water is used to extract the solvent from the gel, and the gel is cooled below the polymers glass transition temperature and freeze-dried under vacuum to produce a nanofibrous scaffold. The scaffolds porous structure (pore size, interconnectivity, porosity) can be controlled by the presence of porogens such as sugar, inorganic salt, and paraffin spheres [8, 29-31, 33]. This fabrication method is relatively simple and offers the scaffold engineer a great amount of

control, however, it is limited to use with a small number of polymers and would be difficult to scale up [34].

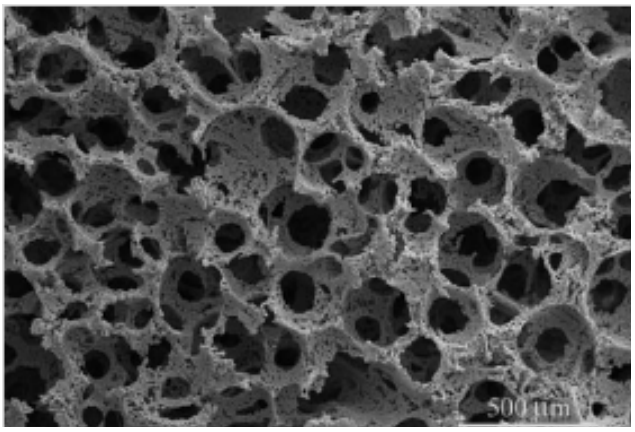

Figure 4. SEM of a PLLA nanofibrous scaffold created through phase separation. Paraffin spheres were used to create pores that ranged in diameter from 250 - 420 µm [33].

Electrospinning

While self-assembly and phase separation both successfully create nanofibrous ECM analogue scaffolds, they are not practical processing techniques. Electrospinning is a simple process requiring little specialized equipment, which can be used in a laboratory setting or easily scaled up for large-scale production. In brief, a polymer is placed in solution and drawn into a syringe fitted with a blunt tip needle. The surface tension of the polymer solution at the tip of the needle is overcome through the application of a large electric potential. A grounded target is placed a set distance from the charged polymer solution to create a static electric field. When the electric potential reaches a critical level,

the electrostatic forces overcome the surface tension at the needle tip, and a fine jet of entangled polymer chains are drawn out. This jet whips through the air toward the grounded target, creating a dry fiber through the evaporation of the polymers solvent. This produces fibers that range from 50 nm to 10 μm in diameter, which are collected on the grounded target [8, 14, 29-31].

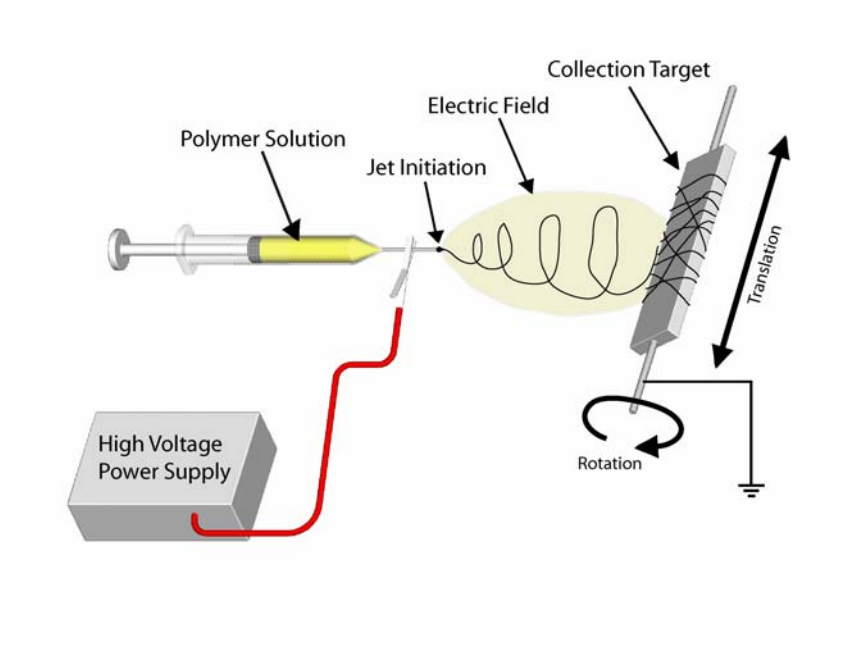

Figure 5. Generic electrospinning setup depicting the major components of the electrospinning process, including a high voltage power supply, polymer solution, and collection target.

As simple as electrospinning is, it offers the tissue engineer the ability to tailor several different aspects of the ECM analogue scaffolds. Fiber diameters can be controlled by altering the concentration of the polymer solution; solutions made of higher concentrations produce larger diameter fibers. Rotating the grounded target can control the alignment of the collected fibers. A high rate of rotation will produce fibers that align

parallel to the direction of rotation, while a low rotational speed will create a fibrous scaffold of randomly aligned fibers [35]. Scaffold thickness is strictly dependant on the volume of solution to be electrospun, while scaffolds of any geometry can be created machining the desired shape into a grounded target.

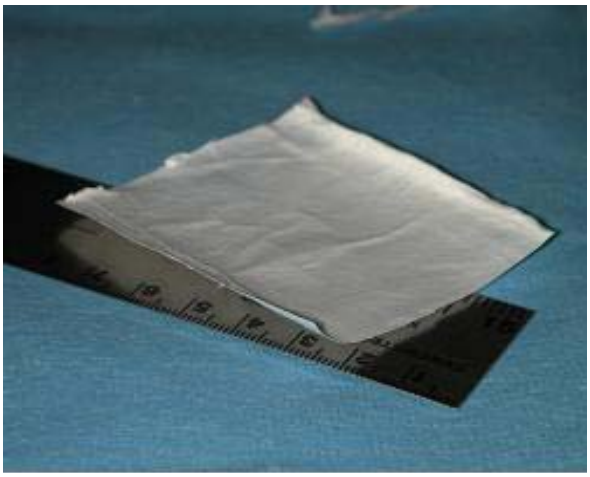

Figure 6. Photograph of large electrospun fibrinogen scaffold [12].

The only aspect of electrospinning that is not easy to directly control is the size of the scaffolds pores. This can be controlled indirectly by creating smaller diameter fibers, as smaller fibers result in smaller, more tightly packed pores [36, 37]. However, it is not possible to alter pore size without changing any of the other electrospinning parameters. This is due to the fact that electrospun scaffolds do not contain true, cylindrical pores like other processing techniques. While electrospun scaffolds have porosities that are on par with scaffolds produced through other techniques, they are merely a group of non-woven fibers lying loosely upon one another. This creates a unique situation that potentially allows for cells to simply move the fibers aside to create a pore diameter of their choosing

as they migrate throughout the scaffold. This dynamic architecture renders the reporting of electrospun scaffold pore diameters unnecessary, as the cells will create a pore as large or small as required [19]. However, this makes the reporting of scaffold porosity and permeability even more important in determining the characteristics of successful electrospun ECM analogues.

Materials and Methods

Electrospinning

Solutions of three different concentrations of fibrinogen (100, 120, and 150 mg/ml) were made with a 90% by volume solution of 1,1,1,3,3,3-hexafluoro-2-propanol (HFP) and 10% by volume 10x MEM in a glass scintillation vial. All reagents were purchased from Sigma Aldrich, Co. Solutions were left overnight on a shaker plate to ensure that all fibrinogen had dissolved and formed a homogenous solution. These solutions were then loaded into a 5 ml Beckton Dickinson syringe and placed in a KD Scientific syringe pump (Model 100) to be dispensed at a rate of 4 ml/h. A high voltage power supply (Spellman CZE1000R; Spellman High Voltage Electronics Corporation) was used to apply a voltage of 25 kV to a blunt tip 18 gauge needle fixed to the solution containing syringe. Solutions were electrospun onto a flat, stainless steel, grounded mandrel (2.5 cm wide × 10.2 cm long × 0.3 cm thick) placed 12 cm from the needle tip and rotating at a rate of ~500 rpm to produce a scaffold of randomly oriented fibers. The same procedure was used in an attempt to produce aligned fiber scaffolds, however the mandrel rotational speed was increased to 3000-4000 rpm. Regardless of whether or not truly aligned fibers were successfully created, scaffolds created with a high mandrel rotational speed were referred to as aligned scaffolds for the sake of simplicity in reporting results. Immediately after

electrospinning, scaffolds were cut from the mandrel and placed in a fume hood for 30 minutes for degassing and removal of remaining HFP.

Scaffold Characterization

Prior to characterization, the dry scaffolds were placed in a desiccation chamber overnight to ensure they were completely free of moisture. These samples were then gold sputter coated (Model 550; Electron Microscope Sciences) in preparation for scanning electron microscopy (JSM-820 JE Electron Microscope; JEOL). A scanning electron micrograph (SEM) of each fibrinogen concentration, both aligned and randomly oriented, was taken at 1500x magnification. These micrographs were then digitized using a flatbed scanner (Hewlett-Packard Scanjet 5550c). Samples of each dry electrospun scaffold were cut from the large mats and placed in phosphate buffered saline for 24 hours. SEMs of these hydrated samples were then taken on an environmental scanning electron microscope (Hitachi S-3400N) in their fully hydrated state at magnifications between 1000 and 1500x. To determine fiber size and pore area, the ImageTool 3.0 image analysis software package was used (Shareware provided by UTHSCSA). The software was calibrated using the micron scale bar of each picture. An average fiber diameter was determined by measuring the diameter of 60 different fibers. Average pore areas were determined by making a short and long axis measurement across 60 different open areas bordered by fibers, averaging these pore diameters, and calculating the area using the formula for the area of a circle.

The same procedure and software were used for SEMs of both the dry and hydrated samples.

Flowmeter Design

Scaffold permeability was measured using a device and method that were modified from the work of Dr. Marcus Carr et al. (figure 7) [28, 38, 39]. This required the design and construction of a flowmeter and specimen mount to measure the amount of fluid passed through a fixed electrospun scaffold area over time. Electrospun scaffolds have high porosities, allowing water to migrate outside of the intended area of fluid flow and into surrounding areas of the scaffold. The bulk of the flowmeter came directly from Dr. Carr's simplistic design, with a 10 ml pipette (Fisher Scientific) used as the scale. To create a larger pressure head and push fluid through the tightly packed electrospun scaffolds faster, the height *h* was increased from 20 cm to 150 cm.

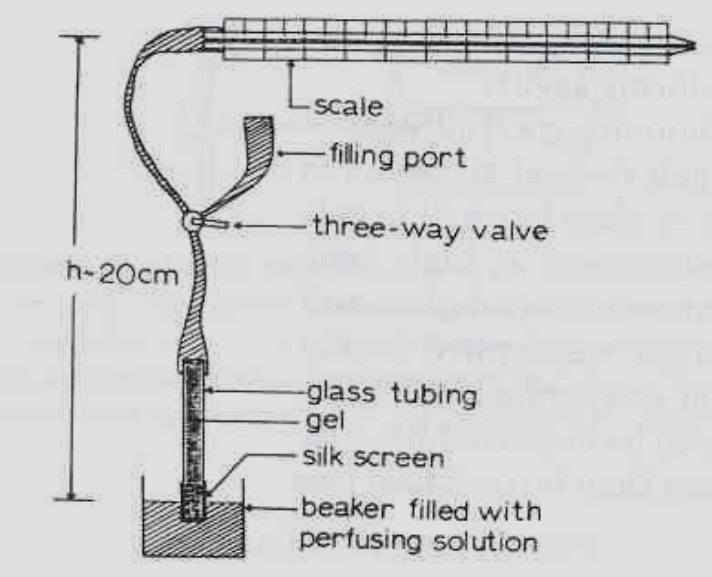

Figure 7. Diagram of a simple flowmeter designed for the measurement of fibrin gel permeability [39].

The specimen-mounting portion of the flowmeter in figure 7 (glass tubing, silk screen) was designed to hold a fibrin gel, and would not support an electrospun scaffold. For this reason a novel specimen mounting apparatus had to be fabricated. To ensure that all fluid traveled through a set area of the electrospun scaffold and produced accurate permeability values, the mounting apparatus was designed to work by compressing the outer edge of the scaffold between two silicone gaskets. The compression was intended to form a tight seal and force all fluid flow through the open center of the specimen mounting apparatus. A large pore metal screen was placed on the underside of the scaffold to prevent excessive distension of the test scaffold, which would again alter the cross sectional area of fluid flow and effect permeability measurement. The completed flowmeter and specimen mount used in permeability testing are shown in figures 8-11, with significant component dimension data contained in table 2.

Figure 8. Photograph of scaffold permeability flowmeter setup, similar to that of Dr. Carr's (figure 7), with a specimen mount designed specifically for electrospun scaffolds.

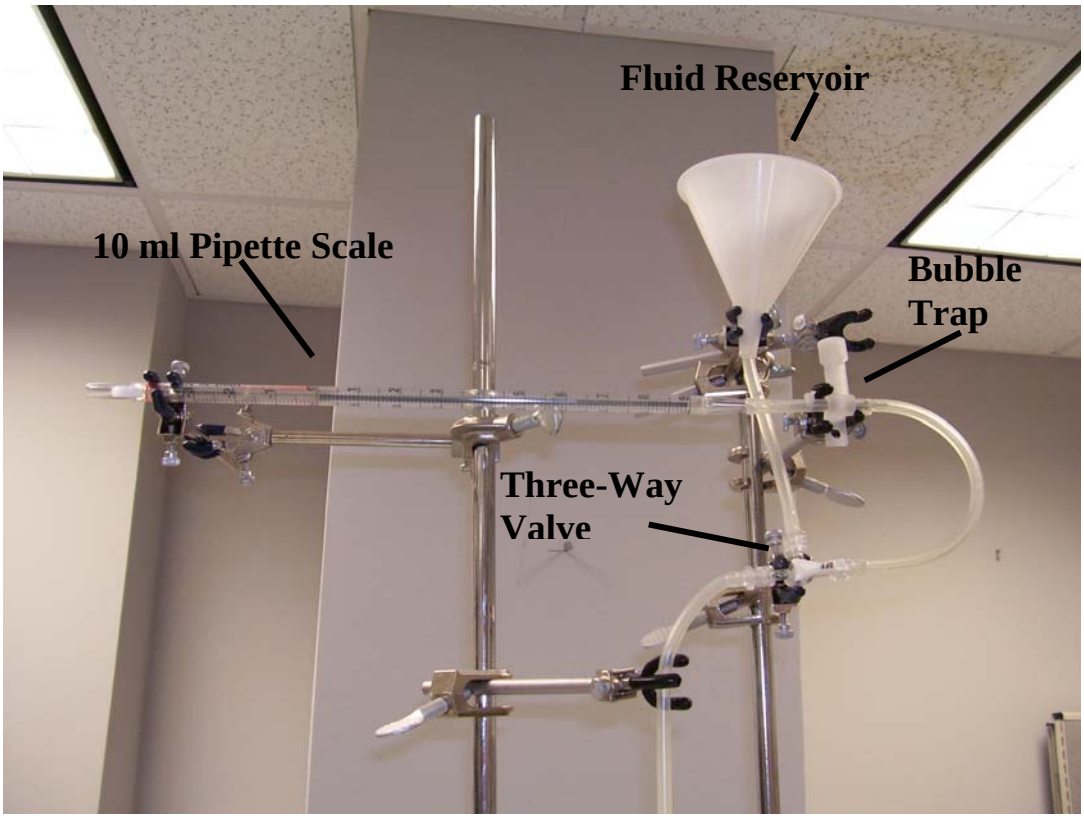

Figure 9. Measurement portion of the scaffold flowmeter. This portion was created to be similar to Dr. Carr's flowmeter, with a 10 ml pipette scale, a fluid reservoir, and three-way valve. A bubble trap was added to remove bubbles from the tubing and make measurement more accurate.

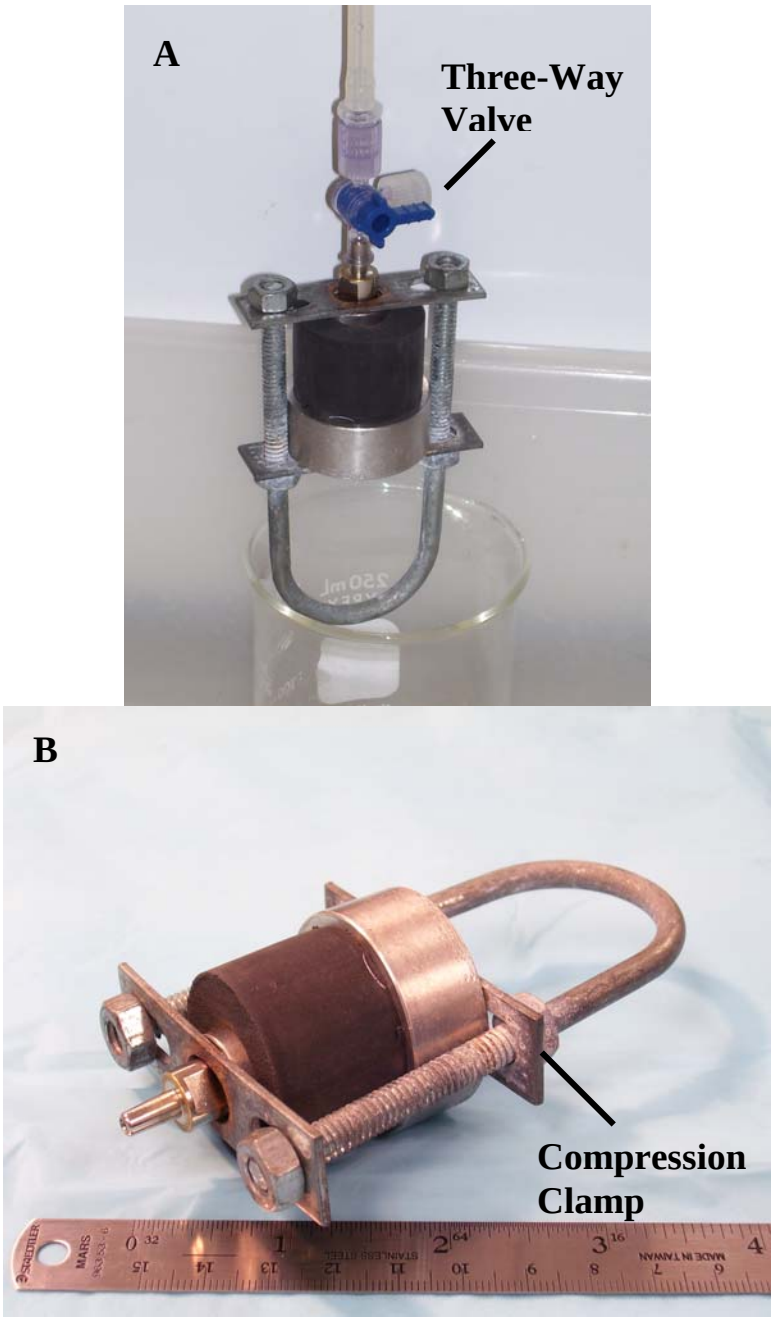

Figure 10. Flowmeter specimen mount attached to a three-way valve to stop/start water flow (A) and free standing to show its size scale while attached to the compression clamp (B).

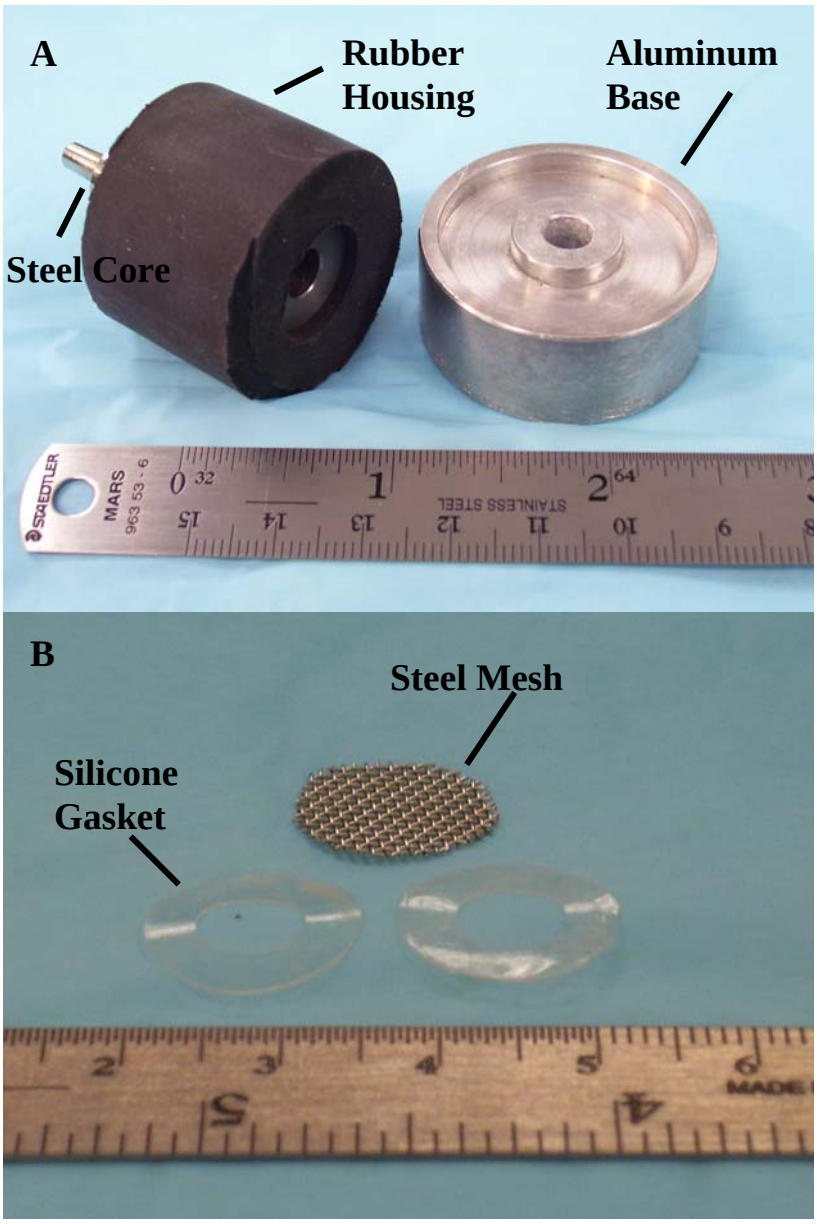

Figure 11. (A) Specimen mount composed of an aluminum base, a stainless steel inner core, and a rubber external housing. (B) To accurately measure permeability, scaffolds are compressed between two silicone gaskets. A steel mesh is then placed beneath the scaffold and gaskets to reduce scaffold distension.

Table 2. Table of specimen mount components, the materials they are constructed from, and their pertinent dimensions. O.D. refers to outer diameter, I.D. refers to inner diameter, and D is simply diameter.

Component	Material	Dimensions
Core	Stainless Steel	2.5 cm high 1.5 cm O.D. 0.75 cm I.D.
Housing	Rubber	2.5 cm high 3.5 cm O.D. 1.5 cm I.D.
Base	Brushed Aluminum	1.5 cm high 3.75 cm O.D. 0.75 cm I.D.
Gaskets	Silicone	0.03 cm thick 1.5 cm O.D. 0.75 cm I.D.
Mesh	Steel	0.06 cm thick 1.5 cm D

Test of Flowmeter Efficacy

In order to test the efficacy of the flowmeter design, in particular the design of the compression based specimen mount, three different fibrinogen scaffolds were electrospun. A randomly oriented scaffold of each concentration whose permeability was to be tested (100 mg/ml, 120 mg/ml, and 150 mg/ml) was created and placed in the specimen mount. The flowmeter and 10 ml pipette were filled with PBS that had been dyed dark red with food coloring in order to stain the areas where fluid passed through the scaffold. The idea being that if the specimen mount functioned correctly, the only fluid flow would take place in the center of the scaffold, dying that region red. The outer edge of the scaffold,

compressed between the two silicone gaskets, should not allow fluid flow and therefore remain mostly dry and un-dyed. Should the specimen mount not create a tight compression seal around the outside of the scaffold, dyed fluid would leak out of the area designated for fluid flow and stain the entirety of the scaffold.

Permeability Measurement

Disks 21 mm in diameter were punched from each of the large dry electrospun mats for permeability testing. They were individually massed and thickness measurements were taken. Prior to permeability testing, the volume fraction of each disk was determined for both dry and hydrated samples using the following equation:

$$Volume\ Fraction = \frac{Calculated\ Scaffold\ Density}{Known\ Material\ Density} \times 100 \qquad (1)$$

The calculated scaffold density was determined by dividing the mass of the scaffold by the total volume of the scaffold, while the density of fibrinogen was known to be 1.38 g/cm^3 [40]. Hydrated samples were soaked for 24 hours in PBS. It has been shown previously in our lab that electrospun fibrinogen scaffolds experience a drastic reduction in diameter when place in aqueous solutions. After 24 hours in PBS, the shrunken diameter and thickness of the samples were measured to determine their wet total volume. The scaffolds previously measured dry mass was then used in the volume fraction equation, as the only difference in mass was due to the addition of water and not a change in the actual scaffold.

Scaffolds both dry and hydrated were individually placed in the specimen mount. The flowmeter tubing and the 10 ml pipette were filled with PBS and permeability testing was begun at room temperature (~25°C). Fluid flow was measured using the incremental marks on the 10 ml pipette and was recorded every minute for the first 10 minutes of testing. After the initial 10 minutes recordings were made at 15 minutes and 20 minutes, in addition the total time for 13 ml (maximum volume of pipette) to pass through the scaffold was recorded. These time values were then used in the following Darcy equation to determine scaffold permeability:

$$\tau = \frac{Q\eta h}{Ftp} \tag{2}$$

Where τ is the scaffolds permeability in darcy's (D), Q is the fluid volume passed through the scaffold in time t, η is the viscosity of the fluid (0.89 cp for waterat 25°C), F is the cross sectional area of the scaffold perpendicular to fluid flow, and p is the applied pressure head [38, 39]. The applied pressure head p was determined by using the following equation:

$$p = \rho g h \tag{3}$$

Where ρ is the density of water (1000 kg/m^3 at 25°C), g is the gravitational force (9.8 m/s^2), and h is the total height of the system in meters (1.5 m). This pressure must then be converted from pascals (Pa) to atmospheres (atm) for use in the Darcy equation.

Permeability Based Fiber Diameter and Pore Size

The permeability values calculated previously were then used to determine the average fiber diameters and pore areas of the electrospun scaffolds for comparison to those values measured with the ImageTool image analysis program. The scaffolds average fiber diameter can be determined from the scaffolds permeability using the following equation:

$$d^2 = k\tau\phi \qquad (4)$$

Where k is a constant whose value is known to be 10, determined from measurements of permeation through irregularly packed metal rods of a known diameter, which has proven appropriate for use with studies of wool, cotton, cellulose fibers, and fibrin gels. For the purpose of this study it has been assumed that the differences in fiber arrangements between electrospun fibrinogen and fibrin gels are negligible, allowing for the use of this constant. The volume fraction of the scaffold is given by ϕ, which was determined prior to permeability testing, and τ is the scaffolds permeability in Darcy's (D). The average pore radius can be determined directly from permeability data as follows:

$$r = 0.5093/\tau^{-1/2} \qquad (5)$$

From this, assuming all pores to be circular for the sake of simplicity, the average pore area can be calculated from the equation for the area of a circle [38].

Statistical Analysis

Statistical analysis was performed on mean fiber diameters and pore sizes of both dry and hydrated scaffolds of differing concentrations and fiber alignments determined through image analysis and found directly by permeability measurement based equations. Permeabilty values were compared among fibrinogen concentrations, fiber alignments, and states of hydration. All statistical analysis was based on a Kruskal–Wallis one-way analysis of variance on ranks and a Tukey–Kramer pairwise multiple comparison procedure ($\alpha = 0.05$, $P < 0.0001$) performed with the JMP®IN 4.0.3 statistical software package (SAS Institute, Inc.). Graphical depictions were constructed with Microsoft Excel 2000.

Results

Scaffold Characterization

As previously stated, the two sets of micrographs were taken with two different scanning electron microscopes, resulting in their difference in appearance (dry scaffolds in figure 12 and hydrated scaffolds in figure 13). All of the dry scaffolds were taken at 1500x, while the hydrated scaffolds were taken between 1000 and 1500x. Fiber diameters ranged from 0.5 to 1.04 μm in diameter and were significantly different between solution concentrations; however, they were not significantly different between fiber orientations, or states of hydration within a single concentration. The major difference between the two sets of scaffolds was in the size of their pores, or void spaces between the fibers. The dry scaffolds contained pores that were clearly visible in the SEMs, while the hydrated scaffolds, particularly the 100 mg/ml concentration, showed very little void space. The hydrated fibers were densely packed leaving little room for pores. Average pore diameters ranged from 0.57 to 3.7 μm, with hydrated pores being significantly smaller than their dry counterparts (table 3).

Despite the disparity in pore size between the two sets of scaffolds, both behaved the same as previously published electrospun data. Fiber diameters increased linearly with electrospun solution concentrations (with R^2 values of 0.9771, 0.9993, 1, and 0.9944 for random/dry, aligned/dry, random/wet, and aligned/wet respectively), and larger diameter fibers resulted in the formation of larger diameter pores (figure 14). In fact, the plot of

average pore diameter versus fibrinogen concentration showed that pore diameter increased linearly with increased concentration in the same way that average fiber diameter increased linearly (with R^2 values of 0.968, 0.9772, 0.8854, and 0.9533 for random/dry, aligned/dry, random/wet, and aligned/wet respectively).

Table 3. Average fiber and pore diameters of electrospun fibrinogen scaffolds determined with ImageTool for both dry and hydrated specimens. All measurements are in μm.

Fibrinogen Concentration	Fiber Orientation	Hydration	Fiber Diameter	Pore Diameter
100 mg/ml	Random	Dry	0.50 ± 0.15	1.88 ± 0.70
100 mg/ml	Aligned	Dry	0.51 ± 0.18	1.80 ± 0.60
100 mg/ml	Random	Hydrated	0.54 ± 0.12	0.61 ± 0.21
100 mg/ml	Aligned	Hydrated	0.55 ± 0.11	0.57 ± 0.22
120 mg/ml	Random	Dry	0.75 ± 0.22	2.77 ± 0.94
120 mg/ml	Aligned	Dry	0.71 ± 0.15	2.81 ± 1.29
120 mg/ml	Random	Hydrated	0.71 ± 0.29	1.06 ± 0.36
120 mg/ml	Aligned	Hydrated	0.70 ± 0.19	1.13 ± 0.32
150 mg/ml	Random	Dry	0.97 ± 0.35	3.48 ± 1.18
150 mg/ml	Aligned	Dry	1.04 ± 0.36	3.70 ± 1.92
150 mg/ml	Random	Hydrated	0.97 ± 0.22	1.25 ± 0.36
150 mg/ml	Aligned	Hydrated	1.00 ± 0.26	1.52 ± 0.43

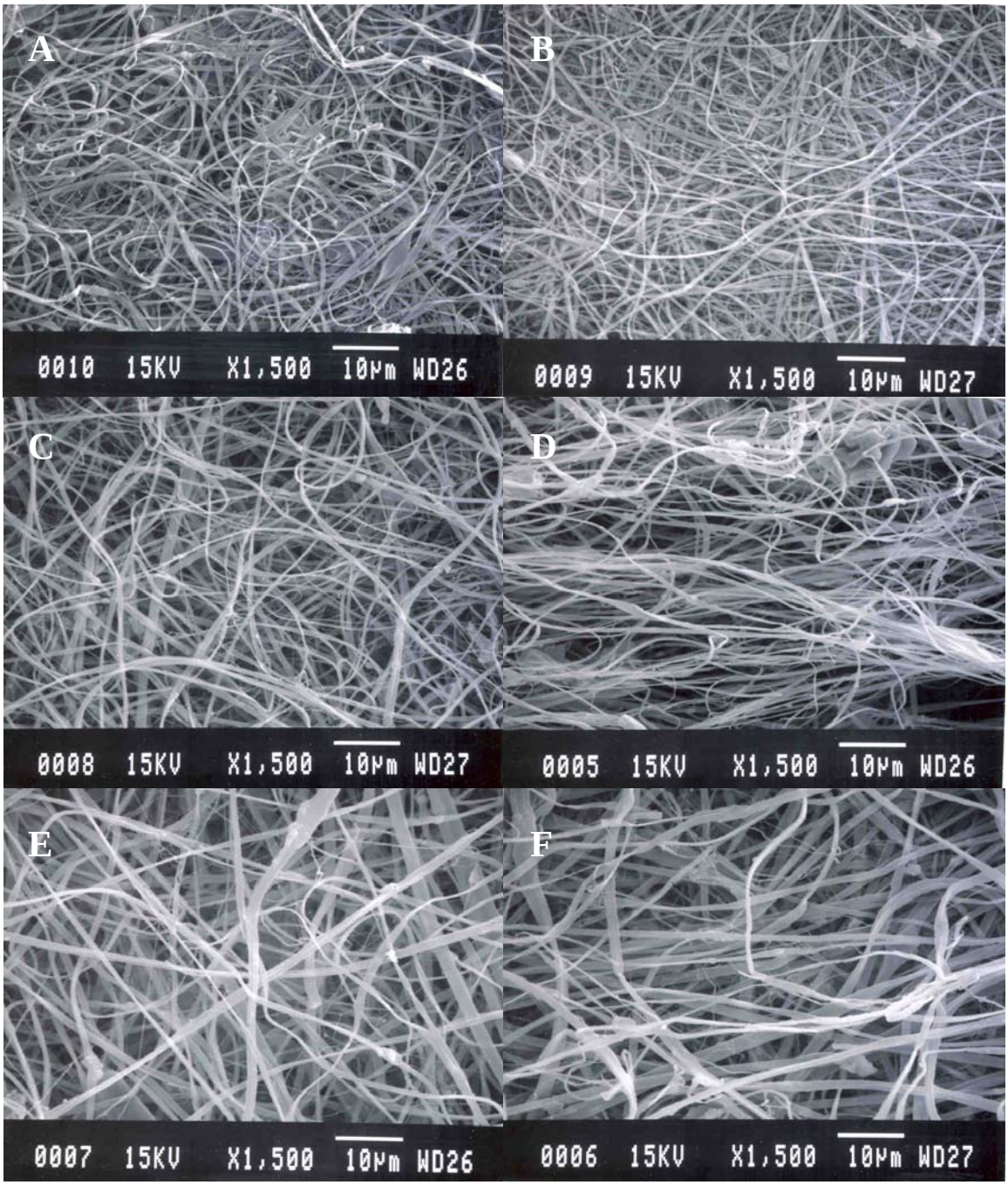

Figure 12. SEMs of dry electrospun fibrinogen scaffolds. The SEMs show scaffolds composed of both randomly oriented fibers (A, C, E) and aligned fibers (B, D, F) of three different concentrations of fibrinogen: 100 mg/ml (A, B), 120 mg/ml (C, D), and 150 mg/ml (E, F). All micrographs were taken at 1500x.

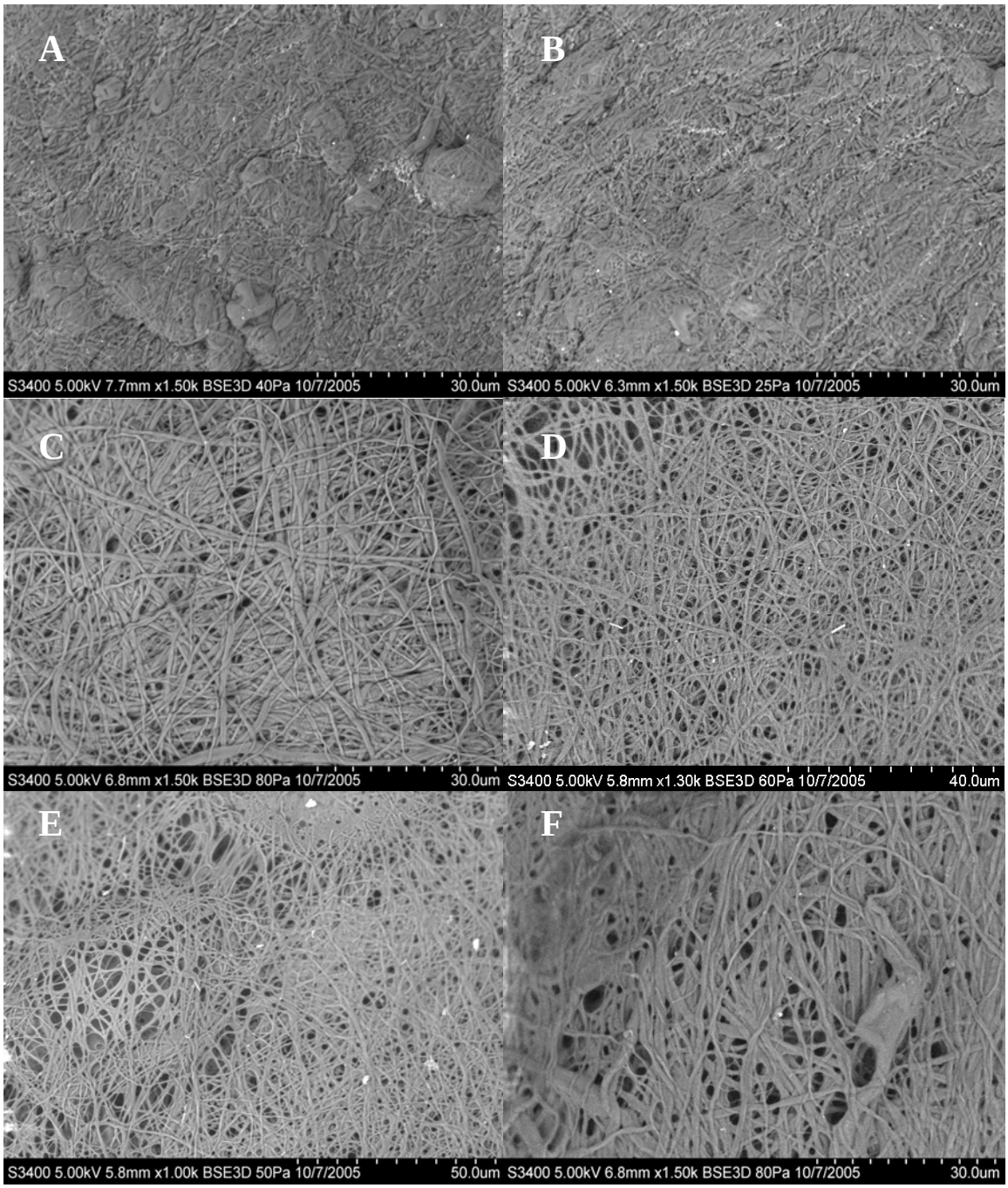

Figure 13. SEMs of electrospun fibrinogen scaffolds hydrated in PBS for 24 hours. Micrographs were taken with an environmental microscope under hydrated conditions at magnifications between 1000 and 1500x. The SEMs show scaffolds composed of both randomly oriented fibers (A, C, E) and aligned fibers (B, D, F) of three different concentrations of fibrinogen: 100 mg/ml (A, B), 120 mg/ml (C, D), and 150 mg/ml (E, F).

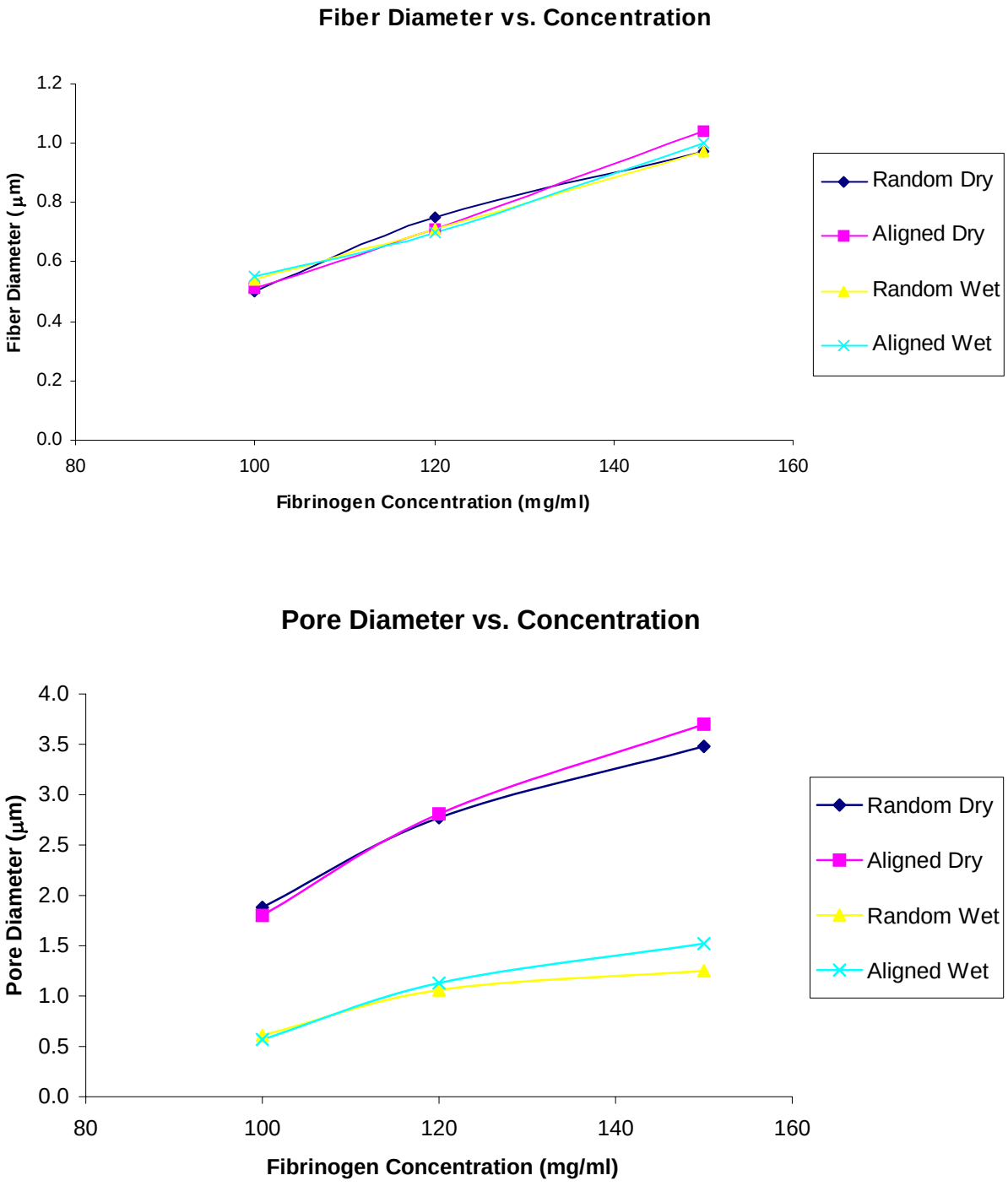

Figure 14. Graphs of fiber (top) and pore (bottom) diameter versus fibrinogen solution concentration. Trendlines were used to determine the linear relationship between the increase of diameter and concentration.

Test of Flowmeter Efficacy

The results of the flowmeter's test of efficacy clearly showed it to work successfully as designed. All three scaffolds tested (100 mg/ml, 120 mg/ml, and 150 mg/ml) revealed a definite dyed circle in their center, indicative of an area of high fluid flow. None of the three showed excessive dying outside of the desired area of fluid flow, proving the compression applied by the specimen mount to be sufficient to resist leaking around the edges, thereby ensuring more accurate permeability measurement.

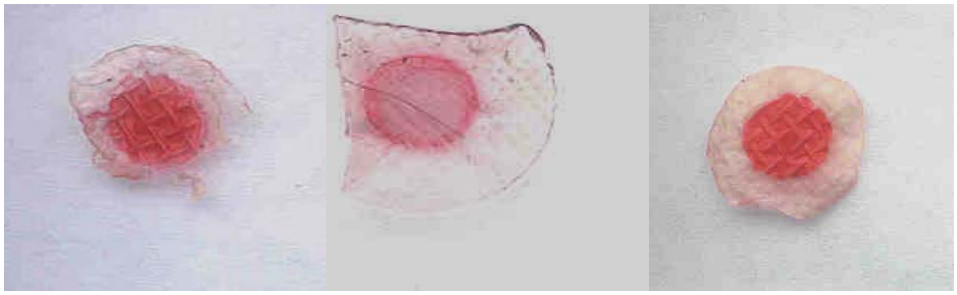

Figure 15. Photographs of electrospun scaffolds of different fibrinogen concentrations (100 mg/ml, 120 mg/ml, and 150 mg/ml from left to right) after 13 ml of dyed PBS had been passed through them to determine the efficacy of the flowmeter's compression based specimen mount.

Permeability Measurement

Prior to permeability testing, the volume fraction of each scaffold was determined for use in the fiber diameter and pore size equations. Overall, the dry scaffolds had relatively low volume fractions that ranged from 12.34 to 19.05 %, indicative of scaffolds

with large amounts of void space. Both of the dry 150 mg/ml concentration scaffolds had significantly greater volume fractions than the other dry scaffolds, with the exception of the 120 mg/ml aligned dry scaffold. The dry 100 mg/ml concentration scaffolds were not significantly different from each other or the 120 mg/ml random dry scaffold. Hydrated scaffold volume fractions ranged from 33.75 to 38.59 %. All hydrated volume fractions were significantly greater than their dry counterparts, but not significantly different from each other. These increased volume fractions corresponded to the SEM images shown previously, which had far reduced pore sizes.

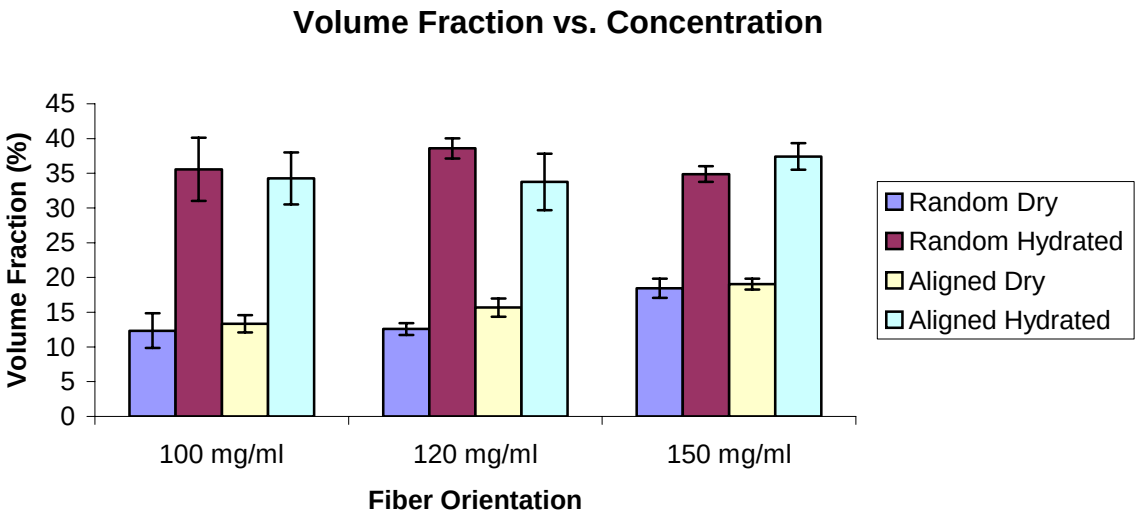

Figure 16. Graph of volume fraction versus fibrinogen solution concentration. Note the increased volume fraction of hydrated samples. As shown previously through SEM analysis, hydrated samples had reduced pore sizes, leading to reduced void space.

Scaffold permeability was recorded every minute for the first ten minutes of the permeability test with results shown in figure 10. Dry permeabilities exhibited very little

change over this time course, the only exception being the randomly oriented 150 mg/ml fibrinogen concentration. This scaffold demonstrated a steady decrease in permeability over the ten-minute duration. Dry scaffold permeability behaved as expected, with lower concentrations that have smaller pore sizes being less permeable than higher concentrations containing larger pores. This trend did not translate to the hydrated scaffolds, which showed the 120 mg/ml concentration to have the highest permeability. Surprisingly, the 150 mg/ml concentration had permeabilities that were closely grouped with those of the 80 mg/ml concentration and less than those of the 120 mg/ml concentration. Again, there was little change in permeability over time for the majority of the scaffolds, with the only exception being the 120 mg/ml randomly oriented scaffold, which exhibited an increase in permeability over time.

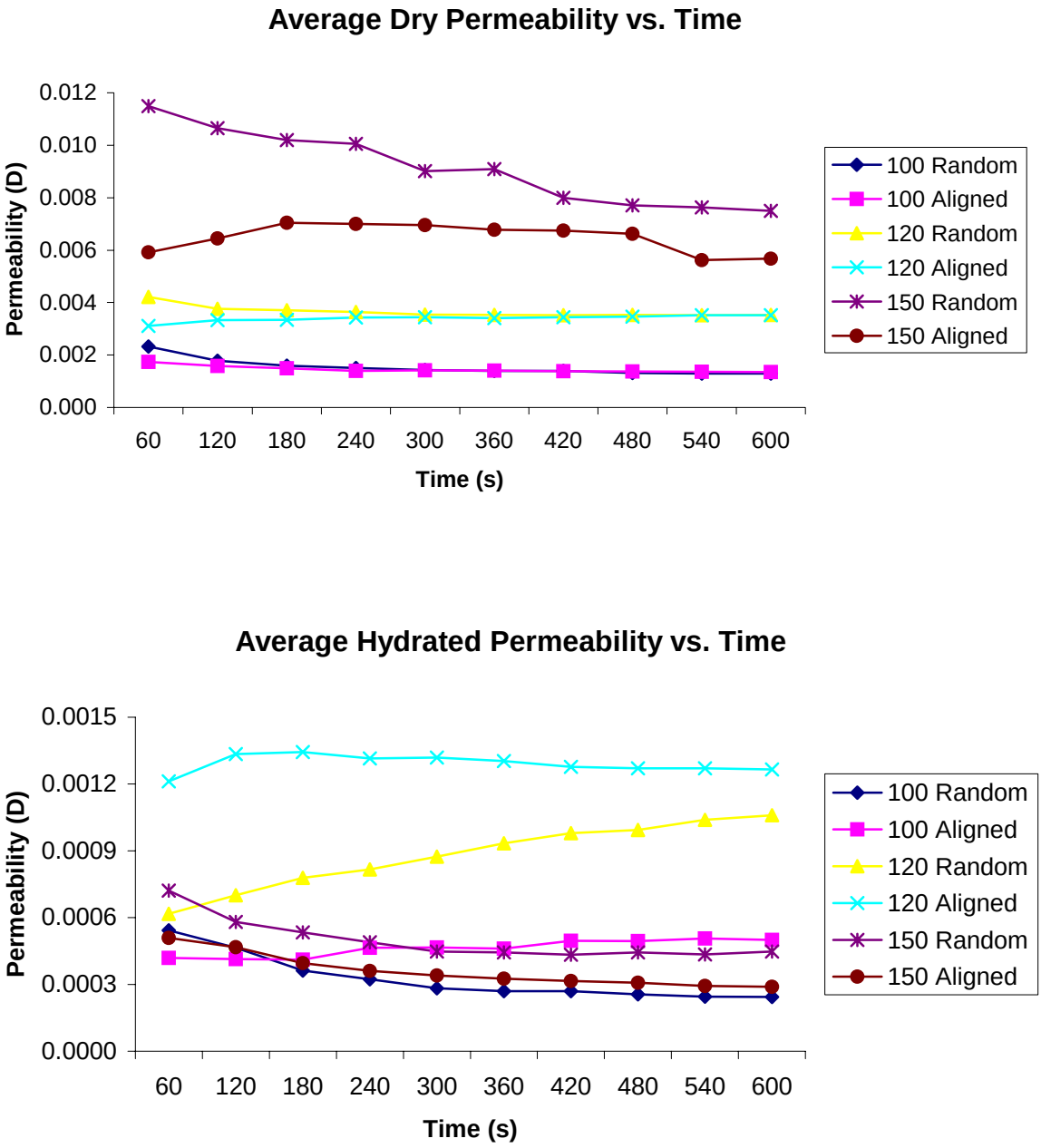

Figure 17. Graphs of average permeability versus time for the first ten minutes of permeability testing for both dry (top) and hydrated (bottom) electrospun fibrinogen samples.

Upon completion of the ten minute timed test, scaffold permeability was measured additionally at 15 minutes, 20 minutes, and finally the total time required for 13 ml to flow through the scaffold was recorded. The permeability was calculated at each time point and and an average permeability was determined (figure 18). Permeabilities ranged from 0.0013 to 0.0092 D for dry scaffolds, and 0.00029 to 0.0012 D for hydrated scaffolds. Dry scaffolds exhibited a definite trend of increased permeability with increased concentration, while hydrated scaffolds were all closely grouped together with no identifiable trend (figure 19). The addition of trendlines revealed that both the randomly oriented dry scaffolds (R^2 value of 0.9828) and the aligned fiber dry scaffolds (R^2 value of 1) had a linear relationship between fibrinogen solution concentration and permeability. The application of a linear trendline to the hydrated scaffolds resulted in extremely low R^2 values, indicating that the linear relationship does not hold true for the hydrated samples due to the permeability of the 150 mg/ml concentration samples being lower than expected.

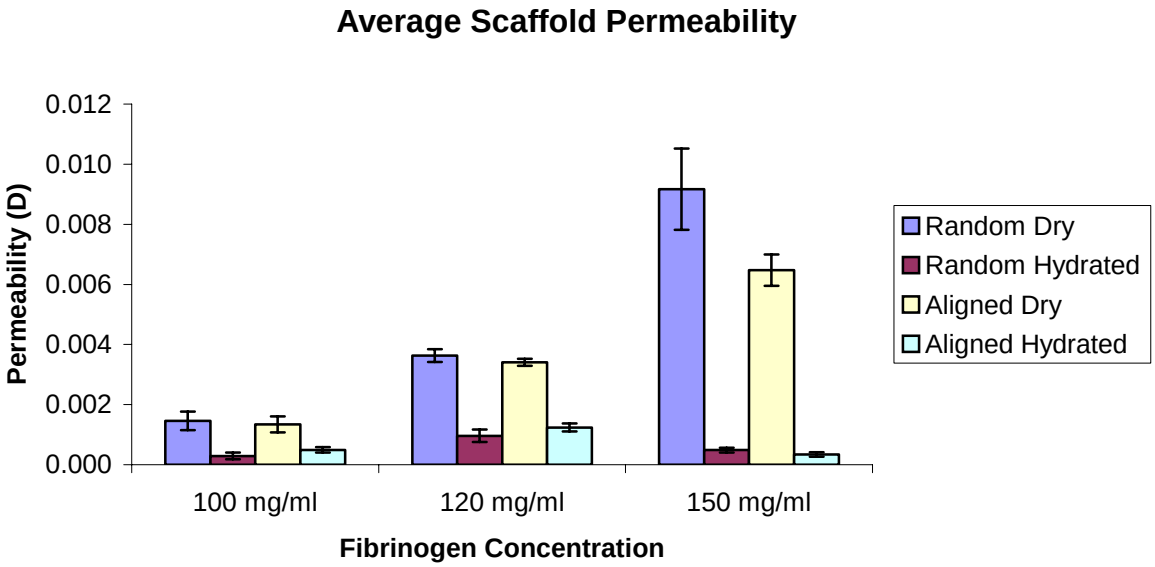

Figure 18. Graph of average scaffold permeability versus fibrinogen concentration. Note the difference between dry and hydrated samples, as well as little change between randomly oriented and aligned fibers.

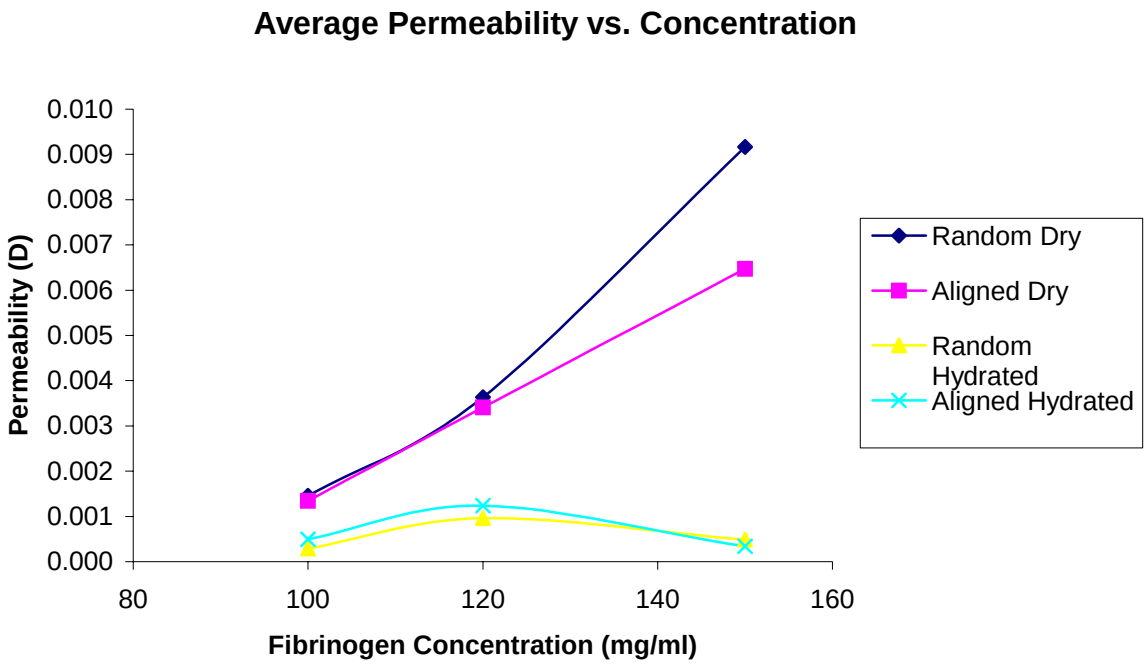

Figure 19. Graph of average permeability versus fibrinogen concentration, depicting the linear relationship between dry scaffold permeability and fibrinogen concentration. Note that the hydrated scaffolds did not exhibit this relationship as the permeability of the 150 mg/ml concentration was lower than expected.

Statistical analysis of average permeability values revealed there to be significant differences between the three fibrinogen concentrations for the dry samples. The 150 mg/ml concentration was significantly larger than the 120 mg/ml concentration, and the 120 mg/ml concentration was significantly larger than the 100 mg/ml concentration. The only difference between fiber orientations was seen with the dry 150 mg/ml concentration where the randomly oriented scaffold had significantly higher permeability than the aligned fiber scaffold. Hydrated scaffolds were not significantly different from one another regardless of concentration or fiber orientation, and were only significantly different from the dry 150 and 120 mg/ml concentrations. Surprisingly, the permeability

of the dry 100 mg/ml concentration scaffolds was small enough to be considered insignificantly different from the hydrated samples.

Permeability Based Fiber Diameter and Pore Size

Having already determined average fiber diameters and pore sizes through ImageTool analysis, the same quantities were calculated using equations 4 and 5. This was done to determine the efficacy of the flowmeter as a tool for scaffold characterization outside of reporting permeability values, and to test the accuracy of the ImageTool software in measuring electrospun scaffolds topographical features. For the most part, average fiber diameter values calculated from scaffold permeability were not statistically different from ImageTool values (figure 20). A complete table of statistical differences is contained in Apendix A for referencing. Average fiber diameters of scaffolds of the 100 mg/ml and 120 mg/ml fibrinogen concentrations were not statistically different between the two measurement methods, or within a single concentration for different fiber orientations, and states of hydration. The fiber diameters of the dry 150 mg/ml concentration scaffolds were not statistically different between measurement methods, or fiber orientations. They were also not significantly different from the hydrated fiber diameters determined through ImageTool. However, there were statistical differences between the aforementioned fiber diameters and the hydrated fiber diameters determined by the permeability based equations. These hydrated fiber diameters were much reduced

due to the extremely low permeability values of the hydrated 150 mg/ml concentration scaffolds.

Table 4. Average fiber and pore diameters of electrospun fibrinogen scaffolds determined by both ImageTool analysis and permeability based calculations. All measurements are in μm.

Fibrinogen Concentration	Fiber Orientation	Hydration	Fiber Diameter (ImageTool)	Pore Diameter (ImageTool)	Fiber Diameter (Permeability)	Pore Diameter (Permeability)
100 mg/ml	Random	Dry	0.50 ± 0.15	1.88 ± 0.70	0.43 ± 0.07	0.039 ± 0.003
100 mg/ml	Aligned	Dry	0.51 ± 0.18	1.80 ± 0.60	0.42 ± 0.09	0.037 ± 0.009
100 mg/ml	Random	Hydrated	0.54 ± 0.12	0.61 ± 0.21	0.29 ± 0.06	0.017 ± 0.004
100 mg/ml	Aligned	Hydrated	0.55 ± 0.11	0.57 ± 0.22	0.40 ± 0.02	0.023 ± 0.001
120 mg/ml	Random	Dry	0.75 ± 0.22	2.77 ± 0.94	0.66 ± 0.06	0.061 ± 0.006
120 mg/ml	Aligned	Dry	0.71 ± 0.15	2.81 ± 1.29	0.71 ± 0.03	0.059 ± 0.001
120 mg/ml	Random	Hydrated	0.71 ± 0.29	1.06 ± 0.36	0.61 ± 0.12	0.031 ± 0.006
120 mg/ml	Aligned	Hydrated	0.70 ± 0.19	1.13 ± 0.32	0.61 ± 0.06	0.035 ± 0.005
150 mg/ml	Random	Dry	0.97 ± 0.35	3.48 ± 1.18	1.34 ± 0.05	0.101 ± 0.007
150 mg/ml	Aligned	Dry	1.04 ± 0.36	3.70 ± 1.92	1.12 ± 0.07	0.082 ± 0.006
150 mg/ml	Random	Hydrated	0.97 ± 0.22	1.25 ± 0.36	0.44 ± 0.03	0.024 ± 0.002
150 mg/ml	Aligned	Hydrated	1.00 ± 0.26	1.52 ± 0.43	0.36 ± 0.02	0.019 ± 0.001

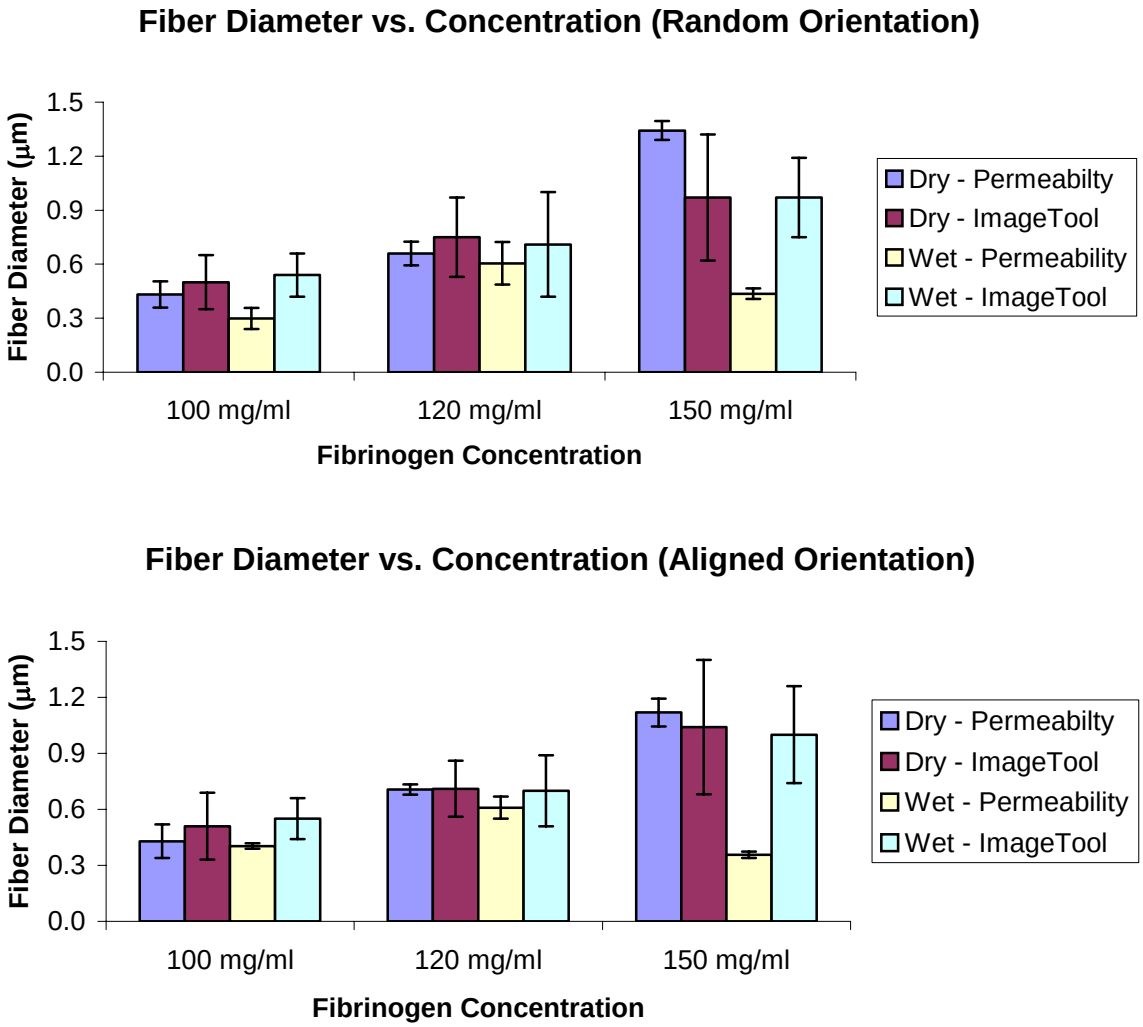

Figure 20. Graph of average fiber diameter versus fibrinogen concentration for randomly oriented (top) and aligned (bottom) scaffolds. Note the significantly reduced values for the hydrated 150 mg/ml concentration scaffolds determined by permeability based equations. These reduced fiber diameter values are due to the extremely low permeability of the hydrated 150 mg/ml scaffolds.

Average pore size measurements (figure 21) proved to be much more diverse than the average fiber diameter measurements. Regardless of concentration, the pore sizes of hydrated scaffolds were significantly smaller than those of dry scaffolds for both methods of measurement. However, unlike average fiber diameter measurements, the two different methods of measurement yielded significantly different pore sizes. Permeability based pore sizes were significantly smaller than pore sizes measured with ImageTool for all fibrinogen concentrations, fiber orientations, and states of scaffold hydration.

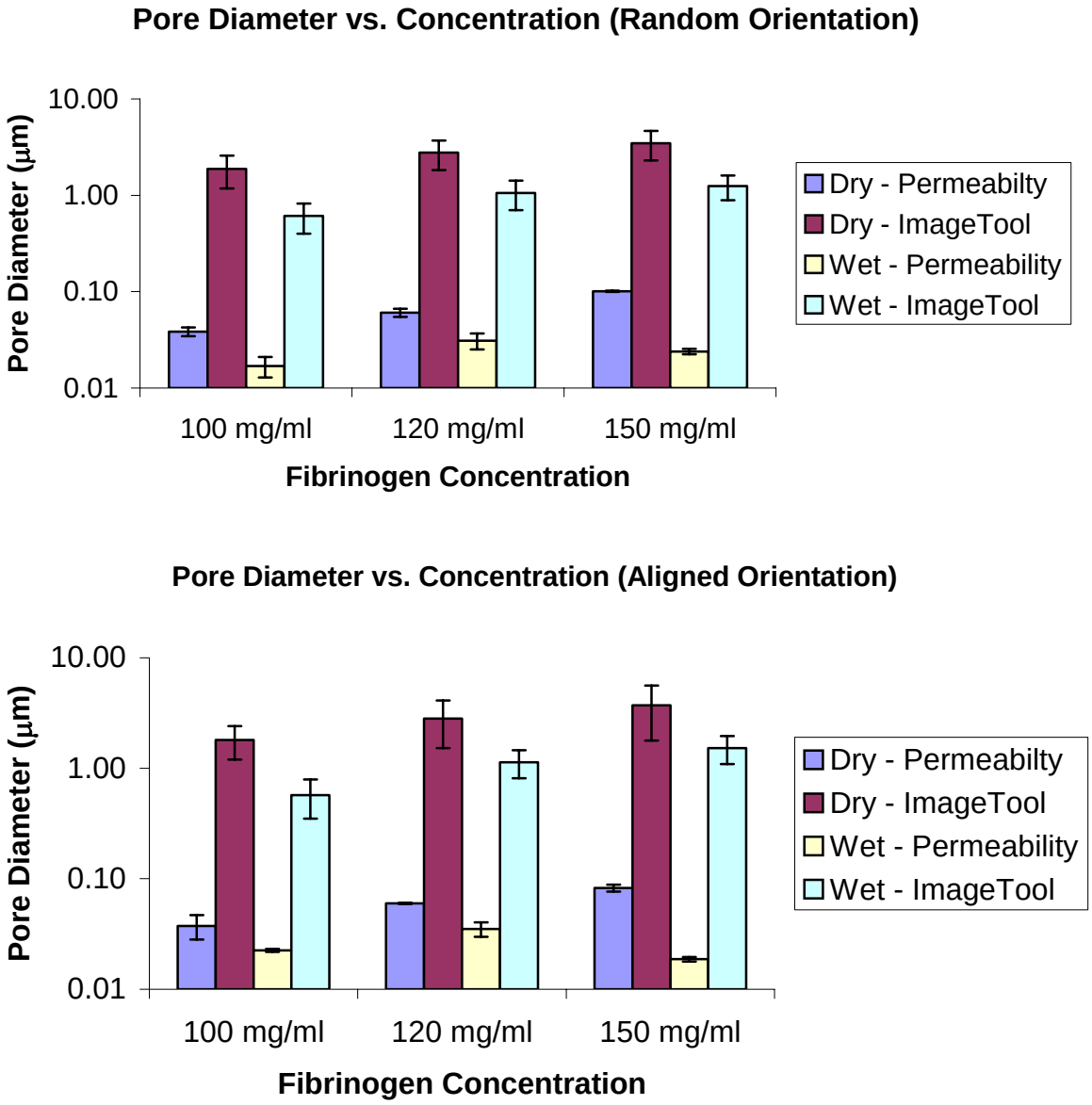

Figure 21. Graph of average pore diameter versus concentration for randomly oriented (top) and aligned (bottom) scaffolds. Note that these graphs are on a log scale, due to the wide discrepancy between dry and hydrated pore diameters.

Discussion

Scaffold Characterization

The trends for both the dry scaffold average fiber and pore diameter values achieved through ImageTool analysis were as anticipated, based upon previously published electrospun data [36, 37]. The results clearly showed fiber diameters to increase linearly with concentration. This is behavior that has been seen in all electrospun scaffolding materials used in this lab, probably due to a relationship between increased solution viscosity and polymer chain entanglements.

Linear increases in pore size with increasing solution concentration were also seen. Previously published data from this lab relied on pore area measurements rather than the pore diameter measurements reported here, making it more difficult to compare the two. Pore area measurement using ImageTool was not done in this study in order to produce values comparable to those produced by the permeability based pore diameter equations. While electrospun scaffolds do not contain true spherical pores, the void spaces present were assumed to be spherical to allow for a diameter to be measured. Regardless, the values obtained for average pore sizes based on ImageTool analysis correspond to the average fiber diameter values reported, as larger diameter fibers result in more space between fibers and more average void space.

As expected, hydrated fibrinogen scaffolds appeared much different than their dry counterparts under SEM examination. Statistical analysis revealed there to be no difference between the dry and hydrated fiber diameters, with significant differences between dry and hydrated pore sizes. Prior to this study, there was question about the hydrated behavior of electrospun fibrinogen. It had been observed with the naked eye that when dry fibrinogen scaffolds were hydrated they almost immediately shrunk in diameter and curled, losing their shape. It was not known if the electrospun fibers were hydrophilic and were swelling by soaking up water, or if they were hydrophobic and tightening in upon themselves. Scaffold characterization with ImageTool made it obvious that fiber diameters did not change, ruling out fiber swelling. Instead, it became apparent that the electrospun scaffolds were extremely hydrophobic, reducing their average pore size by two to three times.

Permeability Measurement

Having seen the results of the SEM image analysis and scaffold characterization, the results of the volume fraction and permeability measurements were somewhat intuitive. As expected, hydrated scaffolds, which visually appeared considerably denser, had significantly higher volume fractions than their dry counterparts. Dry scaffolds had volume fractions that ranged from 12.34 to 19.05 %, while the hydrated scaffolds had volume fractions between 33.75 and 38.59 %.

There are several important pieces of information than can be taken away from this data. Firstly, electrospun scaffolds, in this case dry fibrinogen scaffolds, have extremely high porosities. It is not beyond reason to extrapolate this data to other electrospun polymer scaffolds, as they all form similar structures. This high porosity bodes well for cell migration and nutrient transport, particularly in an electrospun structure where all void spaces are interconnected [17]. While high porosity typically results in poor mechanical properties, electrospun scaffolds of various polymer compositions have proven to be mechanically durable in laboratory testing.

Second, the volume fractions of the hydrated scaffolds were not significantly different from one another while there were differences between dry scaffold volume fractions. It was previously suggested that the decrease in pore size was due to the hydrophobic nature of electrospun fibrinogen. This hydrophobicity caused the scaffolds to densify and contract upon themselves, increasing their volume fraction. However, this contraction ceased at about the same point for each of the different concentrations tested. This would indicate that perhaps a maximum scaffold volume fraction had been achieved, as there were no significant differences between the concentrations. This raises the question: was this a material based limitation or a limitation of the electrospinning process. It may have been that hydrophobic repulsion of the fibrinogen fibers was not capable of further compressing the scaffold, or perhaps fiber movement was limited at a certain point by the overlaying-fiber structure of the scaffold. Further testing will need to be done to determine why higher volume fractions could not be achieved. This may include testing

other hydrophobic electrospun materials, or creating fibrinogen scaffolds with higher dry volume fractions.

The data of permeability versus time for the first ten minutes of testing did not correspond to the trends that were hypothesized. Dry scaffold behavior was closest to the hypothesis that higher concentrations would result in increased permeability, with aligned fiber scaffolds being more permeable than randomly oriented scaffolds. It was also hypothesized that dry scaffold permeability would decrease over time, as the dry scaffold became hydrated and contracted. Testing revealed the 150 mg/ml concentrations had higher permeabilities than the 120 mg/ml, and the 120 mg/ml concentrations had higher permeabilities than the 100 mg/ml concentration. However, there was no difference between randomly oriented and aligned scaffolds, with exception of the 150 mg/ml concentration. In addition, there was no permeability loss over time for the dry scaffolds, with the exception of the dry 150 mg/ml randomly oriented scaffold. This scaffold started with a higher permeability than the dry 150 mg/ml aligned scaffold and became less permeable as time went on. The difference between the 150 mg/ml concentration behavior and the lower two may have been due to the difference in fiber sizes. The larger fibers created by the 150 mg/ml concentration are easier to align than the smaller fibers created by the lesser two concentrations. This may have created a scaffold that was more aligned for the 150 mg/ml concentration, while the smaller 120 mg/ml and 100 mg/ml concentration fibers may have appeared somewhat aligned in SEMs, but not truly aligned throughout the scaffold. These aligned fibers may have created a scaffold of tightly packed fibers, thereby increasing scaffold tortuosity and reducing scaffold permeability. In

addition, the aligned scaffold may have had less room for contraction and fiber reorganization, resulting in a constant permeability compared to the gradual reduction in permeability seen in the randomly oriented scaffold. The restraint of the scaffold within the specimen mount may have played a role in maintaining scaffold permeability over time, as it was anticipated that dry scaffolds would become less permeable as they became more hydrated. However, being pinched firmly between the silicone gaskets the dry scaffolds may not have been able to contract, keeping their permeabilities nearly constant.

In general, the hydrated scaffolds exhibited no change over time and no difference between random and aligned fiber orientations during the first ten minutes of testing. Both the 150 and 100 mg/ml concentrations were closely grouped and nearly constant over time after a small permeability decrease at the outset of testing. The 120 mg/ml concentration exhibited higher permeabilities than the other two concentrations. This time the aligned scaffold was more permeable than the randomly oriented one, while the randomly oriented scaffold gradually increased in permeability until it reached values equivalent to those of the aligned scaffold. There is no explanation for this behavior at this time, as it is quite the opposite of the behavior seen with the other concentrations. Perhaps there were small tears or holes in these scaffolds that propagated as testing took place. Further investigation will need to be performed to explain what caused this behavior, as it may have simply been an aberration, or may have some underlying principle behind it.

Average permeability measurement resulted in trends that for the most part, could have been anticipated based upon the volume fraction and fiber and pore diameter values recorded earlier. Hydrated scaffold permeabilities were significantly less than dry scaffold

permeabilities across the board, as was expected. There were no statistically significant differences between the hydrated scaffold values, reinforcing what was determined earlier, that the hydrated scaffolds had all reached a maximum volume fraction and could not contract further. This maximum scaffold density prevented fluid flow through the scaffold and resulted in minimal permeability. While this does support the earlier findings, it conflicts with the original hypothesis that permeability would increase as fibrinogen concentration was increased. However, the dry scaffolds supported the original hypothesis as there was shown to be a linear relationship between scaffold permeability and fibrinogen concentration. A similar relationship was expected for the hydrated scaffolds, with the 150 mg/ml concentration scaffold exhibiting much higher permeability. There were also differences between the random and aligned fiber orientations that became larger as fibrinogen concentration increased, with the random orientation having larger permeability than the aligned orientation. As explained previously, this may be due to the increasing fiber size of the scaffolds as larger fibers are easier to align.

Permeability Based Fiber Diameter and Pore Size

The reasons for calculating fiber and pore diameters using permeability-based equations were twofold. Firstly, a correlation between the permeability-based fiber diameters and the fiber diameter values obtained through image analysis would confirm the accuracy of the scaffold permeability measurements. Fiber diameters are the easiest

scaffold topographical feature to measure accurately through image analysis, and were therefore the gold standard by which the permeability-based values were compared. Electrospun scaffold pore sizes are extremely difficult to measure accurately with an image analysis program; consequently the values obtained through image analysis were compared to the permeability-based pore sizes upon confirmation of the efficacy of the permeability measurements.

Average fiber diameters were found to be statistically the same for the 100 and 120 mg/ml concentrations, independent of fiber orientation, state of hydration, or method of measurement. Since there was no statistical difference between fiber diameters measured with image analysis software or calculated with permeability-based equations, one could conclude that the permeability flowmeter worked correctly and produced accurate permeability measurements. That being said, the 150 mg/ml concentration fiber diameters calculated with the permeability-based equations were statistically different from those measured with ImageTool. This would indicate that the permeability values for this concentration are incorrect and lower than they should be. This may have also been shown in the permeability versus time data, where the hydrated 150 mg/ml scaffolds had permeabilities comparable to the 100 mg/ml scaffolds. Further permeability testing needs to be performed on scaffolds that do not densify in solution in order to more accurately demonstrate the usefulness of permeability based equations in measuring scaffold fiber diameters.

Results of the average pore size comparison revealed there to be statistically significant differences between all groups, excluding fiber orientation. The pore sizes of

hydrated scaffolds were universally significantly smaller than those of their dry counterparts. However, this result was expected due to the contraction evident in the SEM images when electrospun fibrinogen scaffolds were placed in a PBS solution. This decrease in permeability corresponded to the increase in scaffold volume fraction, and was looked upon as a positive result. The significant differences between methods of measurement raise questions about the accuracy of said methods. Pore sizes calculated with the permeability-based equation were up to 52 times smaller than the pore sizes measured through image analysis. Much like the discrepancy in fiber diameter of the hydrated 150 mg/ml concentration scaffold previously, this challenges the credibility of the permeability-based equations used for calculation. However, unlike in the instance of fiber diameter measurements where only the hydrated 150 mg/ml concentration scaffold produced questionable values, the dry pore sizes were also significantly reduced using calculated values. Dry scaffold permeability was not questioned previously as it fit nicely into a linear relationship between permeability and fibrinogen concentration. This would lead one to believe that the dry pore sizes calculated from the permeability-based equation were correct, and the values measured with ImageTool were incorrect. It could then be assumed that the calculated hydrated pore sizes were also correct, completely discrediting the use of ImageTool as a pore size measurement device. Nevertheless, further testing will need to be performed on electrospun scaffolds that do not contract and alter their volume fractions prior to retiring the ImageTool program from pore size measurement.

Conclusion

This major outcome of this study was the creation of a permeability flowmeter and specimen mount that could accurately and efficiently measure the permeability of electrospun scaffolds. The use of this flowmeter demonstrated a linear relationship between dry scaffold permeability and electrospun solution concentration. Calculation of scaffold volume fractions led to the conclusion that electrospun fibrinogen is extremely hydrophobic and upon immersion in water contracts upon itself, resulting in a significant increase in scaffold volume fraction. This densification results in significantly reduced scaffold permeability. The fibrinogen scaffolds contracted until a maximum volume fraction was reached. This volume fraction was nearly constant for all electrospun concentrations, and led to hydrated scaffold permeabilities that were not significantly different from one another. As electrospun fibrinogen scaffolds are ultimately intended for use as *in vivo* ECM analogue scaffolds, their wetting is inevitable. This wetting will cause their contraction and densification. As shown through previous studies, this densification should not effect cellular penetration into and migration through the scaffolds. However, this densification will also reduce the permeability of the scaffold resulting in decreased nutrient and waste diffusion throughout the scaffold. This lack of proper diffusion may further limit electrospun fibrinogen scaffold thickness and hamper its ability to sustain cellular life.

Additionally, permeability-based equations were used to calculate average fiber diameters and pore sizes. These calculated values were compared to values measured with the ImageTool image analysis software. Fiber diameter comparison resulted in values that were statistically the same for both methods. As fiber diameter measurement is both relatively easy and accurate with the ImageTool software, this demonstrated the ability for a permeability-based equation to produce accurate fiber diameter results. It also proved the accuracy of the flowmeter in measuring electrospun scaffold permeability. Pore diameter comparisons brought the ineptitude of ImageTool as a pore size measurement device to light, as measurements made with ImageTool were up to 52 times larger than those calculated from the permeability-based equation. The problem may not be with ImageTool as a program, as it just measures linear distances on a picture. The problem may be that electrospun scaffolds do not contain pores in the true sense of the word, leading to the measurement of unbounded void spaces. Electrospun scaffolds are merely a collection of nanoscale fibers lying loosely amongst each other, forming what appear to be three-dimensional bounded void spaces on two-dimensional SEMs. In fact, these faux-pores may not be bounded on all sides, instead being several unbounded layers on top of each other. For this reason, the use of permeability-based pore size measurement, which is determined by fluid traveling the path of least resistance through the scaffold, increases the accuracy of pore size reporting.

Literature Cited

Literature Cited

1. Heineken, F.G., and R. Skalak, *Tissue Engineering: A Brief Overview.* Journal of Biomechanical Engineering, 1991. **113**: p. 111.

2. Palsson, B.O., and Sangeeta N. Bhatia, *Tissue Engineering*. 2004, Upper Sadle River, New Jersey: Pearson Prentice Hall.

3. Vacanti, J.P., and Charles A. Vacanti, *The Challenge of Tissue Engineering*, in *Principles of Tissue Engineering*, R. Lanza, Robert Langer, and William Chick, Editor. 1997, R.G. Landes Company. p. 1-5.

4. Langer, R., and Joseph P. Vacanti, *Tissue Engineering.* Science, 1993. **260**: p. 920-925.

5. Bell, E., *Tissue Engineering: A Perspective.* Journal of Cellular Biochemistry, 1991. **45**: p. 239-241.

6. Martins-Green, M., *The Dynamics of Cell-ECM Interactions with Implications for Tissue Engineering*, in *Principles of Tissue Engineering*, R. Lanza, Robert Langer, and William Chick, Editor. 1997, R. G. Landes Company. p. 23-46.

7. Agrawal, C.M., Robert B. Ray, *Biodegradable polymeric scaffolds for musculoskeletal tissue engineering.* Journal of Biomedical Materials Research, 2001. **55**(2): p. 141-150.

8. Boland, E.D., Paul G. Espy, and Gary L. Bowlin, *Tissue Engineering Scaffolds*, in *Encyclopedia of Biomaterials and Biomedical Engineering*, G. Wnek, and Gary Bowlin, Editor. 2004, Marcel Dekker, Inc.: New York. p. 1-9.

9. Zong, X., Harold Bien, Chiung-Yin Chung, Lihong Yin, Dufei Fang, Benjamin S. Hsiao, Benjamin Chu, and Emilia Entcheva, *Electrospun fine-textured scaffolds for heart tissue constructs.* Biomaterials, 2005. **26**: p. 5330-5338.

10. Matthews, J.A., David G. Simpson, Gary E. Wnek, and Gary L. Bowlin, *Electrospinning of collagen nanofibers.* Biomacromolecules, 2002. **3**: p. 232-238.

11. Sell, S.A., Michael J. McClure, Catherine P. Barnes, Danielle C. Knapp, Beat H. Walpoth, David G. Simpson, and Gary L. Bowlin, *Electrospun polydioxanone-elastin blends: potential for bioresorbable vascular grafts.* Biomedical Materials, 2006. **1**: p. 72-80.

12. Wnek, G.E., Marcus E. Carr, David G. Simpson, and Gary L. Bowlin, *Electrospinning of Nanofiber Fibrinogen Structures.* Nano Letters, 2003. **3**(2): p. 213-216.

13. Mooney, D.J., and Robert S. Langer, *Engineering Biomaterials for Tissue Engineering: The 10 - 100 Micron Size Scale*, in *Tissue Engineering*, B. Palsson, Jeffrey A. Hubbell, Robert Plonsey, and Joseph D. Bronzino, Editor. 2000, CRC Press.

14. Norman, J.J., and Tejal A. Desai, *Methods for Fabrication of Nanoscale Topography for Tissue Engineering Scaffolds.* Annals of Biomedical Engineering, 2006. **34**(1): p. 89-101.

15. Venugopal, J., and S. Ramakrishna, *Applications of Polymer Nanofibers in Biomedicine and Biotechnology.* Applied Biochemistry and Biotechnology, 2005. **125**: p. 147-157.

16. Berry, C.C., Gordon Campbell, Antonio Spadiccino, Mary Robertson, Adam S.G. Curtis, *The influence of microscale topography on fibroblast attachment and motility.* Biomaterials, 2004. **25**: p. 5781-5788.

17. Telemeco, T.A., C. Ayres, G. L. Bowlin, G. E. Wnek, E. D. Boland, N. Cohen, C. M. Baumgarten, J. Matthews, and D. G. Simpson, *Regulation of cellular infiltration into tissue engineering scaffolds composed of submicron diameter fibrils produced by electrospinning.* Acta Biomaterialia, 2005. **1**(4): p. 377-385.

18. Levesque, S.G., Ryan M. Lim, and Molly S. Shoichet, *Macroporous interconnected dextran scaffolds of controlled porosity for tissue-engineering applications.* Biomaterials, 2005. **26**: p. 7436-7446.

19. Karande, T.S., Joo L. Ong, and C. Mauli Agrawal, *Diffusion in Musculoskeletal Tissue Engineering Scaffolds: Design Issues Related to Porosity, Permeability, Architecture, and Nutrient Mixing.* Annals of Biomedical Engineering, 2004. **32**(12): p. 1728-1743.

20. Li, S., Joost R. De Wijn, Jiaping Li, Pierre Layrolle, and Klaas De Groot, *Macroporous Biphasic Calcium Phosphate Scaffold with High Permeability/Porosity Ratio.* Tissue Engineering, 2003. **9**(3): p. 535-548.

21. Kannan, R.Y., Henryk J. Salacinski, Kevin Sales, Peter Butler, and Alexander M. Seifalian, *The roles of tissue engineering and vascularisation in the development of micro-vascular networks: a review.* Biomaterials, 2005. **26**: p. 1857-1875.

22. Griffith, C.K., Cheryl Miller, Richard C. A. Sainson, Jay W. Calvert, Noo Li Jeon, Christopher C. W. Hughes, and Steven C. George, *Diffusion Limits of an in Vitro Thick Prevascularized Scaffold.* Tissue Engineering, 2005. **11**(1/2): p. 257-266.

23. Sander, E.A., and Eric A. Nauman, *Permeability of Musculoskeletal Tissues and Scaffolding Materials: Experimental Results and Theoretical Predictions.* Critical Reviews in Biomedical Engineering, 2003. **31**(1): p. 1-26.

24. Mooney, D.J., C. L. Mazzoni, C. Breuer, K. McNamara, D. Hern, J. P. Vacanti, and R. Langer, *Stabilized polyglycolic acid fibre-based tubes for tissue engineering.* Biomaterials, 1996. **17**(2): p. 115-124.

25. Widmer, M.S., Puneet K. Gupta, Lichun Lu, Rudolf K. Meszlenyi, Gregory R. D. Evans, Keith Brandt, Tom Savel, Ali Gurlek, Charles W. Patrick Jr., and Antonios G. Mikos, *Manufacture of porous biodegradable polymer conduits by an extrusion process for guided tissue regeneration.* Biomaterials, 1998. **19**: p. 1945-1955.

26. Mikos, A.G., Georgios Sarakinos, Susan M. Leite, Joseph P. Vacanti, and Robert Langer, *Laminated three-dimensional biodegradable foams for use in tissue engineering.* Biomaterials, 1993. **14**(5): p. 323-330.

27. Mikos, A.G., Michelle D. Lyman, Lisa E. Freed, and Robert Langer, *Wetting of poly(L-lactic acid) and poly(DL-lactic-co-glycolic acid) foams for tissue culture.* Biomaterials, 1994. **15**(4): p. 55-58.

28. Wang, H., Jeroen Pieper, Fabienne Peters, Clemens A. van Blitterswijk, and Evert N. Lamme, *Synthetic scaffold morphology controls human dermal connective tissue formation.* Journal of Biomedical Materials Research, 2005. **74A**: p. 523-532.

29. Smith, L.A., and P. X. Ma, *Nano-fibrous scaffolds for tissue engineering.* Colloids and Surfaces. B: Biointerfaces, 2004. **39**: p. 125-131.

30. Ma, Z., Masaya Kotaki, Ryuji Inai, and Seeram Ramakrishna, *Potential of Nanofiber Matrix as Tissue-Engineering Scaffolds.* Tissue Engineering, 2005. **11**(1/2): p. 101-109.

31. Wen, X., Donglu Shi, and Ning Zhang, *Applications of Nanotechnology in Tissue Engineering*, in *Handbook of Nanostructured Biomaterials and Their Applications in Nanobiotechnology*, H.S. Nalwa, Editor. 2005, American Scientific Publishers: Stevenson Ranch, CA. p. 1-23.

32. Hartgerink, J.D., Elia Beniash, and Samuel I. Stupp, *Peptide-amphiphile nanofibers: A versatile scaffold for the preparation of self-assembling materials.* PNAS, 2002. **99**(8): p. 5133-5138.

33. Chen, V.J., and Peter X. Ma, *Nano-fibrous poly(L-lactic acid) scaffolds with interconnected spherical macropores.* Biomaterials, 2004. **25**: p. 2065-2073.

34. Jayaraman, K., M. Kotaki, Y. Zhang, X. Mo, and S. Ramakrishna, *Recent advances in polymer nanofibers.* Journal of Nanoscience and Nanotechnology, 2004. **4**: p. 52-65.

35. Boland, E.D., Gary E. Wnek, David G. Simpson, Kristin J. Pawlowski, and Gary L. Bowlin, *Tailoring Tissue Engineering Scaffolds Using Electrostatic Processing Techniques: A Study of Poly(Glycolic Acid) Electrospinning.* Journal of Macromolecular Science. Part A: Pure and Applied Chemistry, 2001. **A38**(12): p. 1232-1243.

36. Boland, E.D., Branch D. Coleman, Catherine P. Barnes, David G. Simpson, Gary E. Wnek, and Gary L. Bowlin, *Electrospinning polydioxanone for biomedical applications.* Acta Biomaterialia, 2005. **1**: p. 115-123.

37. Ayres, C., Gary L. Bowlin, Scott C. Henderson, Leander Taylor, Jackie Shultz, John Alexander, Todd A. Telemeco, and David G. Simpson, *Modulation of anisotropy in electrospun tissue-engineering scaffolds: Analysis of fiber alignment by the fast Fourier transform.* Biomaterials, 2006. **Article in Press**.

38. Carr Jr., M.E., and Cara L. Hardin, *Fibrin has larger pores when formed in the presence of erythrocytes.* American Journal of Physiology, 1987. **253**: p. H1069-H1073.

39. Carr Jr., M.E., Linus L. Shen, and Jan Hermans, *Mass-Length Ratio of Fibrin Fibers from Gel Permeation and Light Scattering.* Biopolymers, 1977. **16**: p. 1-15.

40. McManus, M.C., Eugene D. Boland, Harry P. Koo, Catherine P. Barnes, Kristin J. Pawlowski, Gary E. Wnek, David G. Simpson, and Gary L. Bowlin, *Mechanical properties of electrospun fibrinogen structures.* Acta Biomaterialia, 2006. **2**: p. 19-28.

APPENDIX A

Fiber	150 R/D (P)	150 A/D (P)	150 R/H (P)	150 A/H (P)	150 R/D (IT)	150 A/D (IT)	150 R/H (IT)	150 A/H (IT)	120 R/D (P)	120 A/D (P)	120 R/H (P)	120 A/H (P)	120 R/D (IT)	120 A/D (IT)	120 R/H (IT)	120 A/H (IT)	100 R/D (P)	100 A/D (P)	100 R/H (P)	100 A/H (P)	100 R/D (IT)	100 A/D (IT)	100 R/H (IT)	100 A/H (IT)
150 R/D (P)			*	*					*		*	*	*	*	*	*	*	*	*	*	*	*	*	*
150 A/D (P)			*	*													*	*	*	*	*	*	*	*
150 R/H (P)	*	*			*	*	*	*																
150 A/H (P)	*	*			*	*	*	*																
150 R/D (IT)			*	*									*	*	*	*	*	*	*	*	*	*	*	*
150 A/D (IT)			*	*									*	*	*	*	*	*	*	*	*	*	*	*
150 R/H (IT)			*	*									*	*	*	*	*	*	*	*	*	*	*	*
150 A/H (IT)			*	*									*	*	*	*	*	*	*	*	*	*	*	*
120 R/D (P)	*																							
120 A/D (P)																								
120 R/H (P)	*																							
120 A/H (P)	*																							
120 R/D (IT)	*				*	*	*	*													*	*		
120 A/D (IT)	*				*	*	*	*													*			
120 R/H (IT)	*				*	*	*	*																
120 A/H (IT)	*				*	*	*	*																
100 R/D (P)	*	*			*	*	*	*																
100 A/D (P)	*	*			*	*	*	*																
100 R/H (P)	*	*			*	*	*	*																
100 A/H (P)	*	*			*	*	*	*																
100 R/D (IT)	*	*			*	*	*	*					*	*										
100 A/D (IT)	*	*			*	*	*	*					*											
100 R/H (IT)	*	*			*	*	*	*																
100 A/H (IT)	*	*			*	*	*	*																

Table of statistical differences between average fiber diameters of three different fibrinogen concentrations with either random (R) or aligned (A) fibers in either a dry (D) or hydrated (H) state. Diameters were determined through either ImageTool (IT) or use of a permeability-based equation (P). The presence of an '*' indicates a significant difference between the column and row headers.

Pore	150 R/D (P)	150 A/D (P)	150 R/H (P)	150 A/H (P)	150 R/D (IT)	150 A/D (IT)	150 R/H (IT)	150 A/H (IT)	120 R/D (P)	120 A/D (P)	120 R/H (P)	120 A/H (P)	120 R/D (IT)	120 A/D (IT)	120 R/H (IT)	120 A/H (IT)	100 R/D (P)	100 A/D (P)	100 R/H (P)	100 A/H (P)	100 R/D (IT)	100 A/D (IT)	100 R/H (IT)	100 A/H (IT)
150 R/D (P)					*	*							*	*										
150 A/D (P)					*	*							*	*										
150 R/H (P)					*	*							*	*										
150 A/H (P)					*	*							*	*										
150 R/D (IT)		*	*	*			*	*	*	*	*	*	*	*	*		*	*	*	*	*	*	*	*
150 A/D (IT)			*	*	*		*	*	*	*	*	*	*	*	*	*	*	*	*	*	*	*	*	*
150 R/H (IT)					*	*							*	*										
150 A/H (IT)					*	*							*	*									*	*
120 R/D (P)					*	*							*	*										
120 A/D (P)					*	*							*	*										
120 R/H (P)					*	*							*	*										
120 A/H (P)					*	*							*	*										
120 R/D (IT)	*		*	*	*	*	*	*	*	*	*	*			*	*	*	*	*	*		*	*	*
120 A/D (IT)		*	*	*		*	*	*	*	*	*	*			*	*	*	*	*	*	*	*	*	*
120 R/H (IT)					*	*							*	*							*			
120 A/H (IT)					*	*							*	*										
100 R/D (P)					*	*							*	*										
100 A/D (P)					*	*							*	*										
100 R/H (P)					*	*							*	*										
100 A/H (P)					*	*							*	*										
100 R/D (IT)					*	*								*	*								*	*
100 A/D (IT)					*	*							*	*									*	*
100 R/H (IT)					*	*		*					*	*							*	*		
100 A/H (IT)					*	*		*					*	*							*	*		

Table of statistical differences between average pore sizes of three different fibrinogen concentrations with either random (R) or aligned (A) fibers in either a dry (D) or hydrated (H) state. Diameters were determined through either ImageTool (IT) or use of a permeability-based equation (P). The presence of an '*' indicates a significant difference between the column and row headers.

VITA

Scott Allen Sell was born in LaCrosse, WI on April 8, 1981. He moved to Chesterfield, VA, a suburb of Richmond, as a boy and attended Manchester High School, from which he graduated in 1999. He received a Bachelors of Science degree in Biomedical Engineering from Virginia Commonwealth University in the spring of 2003, and began his graduate work at VCU in the fall of that same year.